Immunity 25, 583–594, October 2006 ©2006 Elsevier Inc. DOI 10.1016/j.immuni.2006.07.016

Activation of Leukocyte β_2 Integrins by Conversion from Bent to Extended Conformations

Noritaka Nishida,[1,2,5] Can Xie,[1,2,5] Motomu Shimaoka,[1,3] Yifan Cheng,[4] Thomas Walz,[4] and Timothy A. Springer[1,2,*]
[1] CBR Institute for Biomedical Research
[2] Department of Pathology
[3] Department of Anesthesia
Harvard Medical School
200 Longwood Avenue
Boston, Massachusetts 02115
[4] Department of Cell Biology
Harvard Medical School
240 Longwood Avenue
Boston, Massachusetts 02115

Summary

We used negative stain electron microscopy (EM) to examine the conformational changes in the ectodomains required for activation of the leukocyte integrins $\alpha_X\beta_2$ and $\alpha_L\beta_2$. They transitioned between a bent conformation and two extended conformations in which the headpiece was in either a closed or an open state. Extended integrins exhibited marked flexibility at the α subunit genu and between integrin epidermal growth factor-like (I-EGF) domains 1 and 2. A clasp to mimic juxtamembrane association between the integrin α and β subunits stabilized the bent conformation strongly for $\alpha_X\beta_2$ and less so for $\alpha_L\beta_2$. A small molecule allosteric antagonist induced the extended, open headpiece conformation. A Fab known to activate β_2 integrins on leukocytes induced extension, and a Fab reporter of activation bound only after extension had been induced. The results establish an intimate relationship between extension of β_2 integrins and their activation in immune responses and leukocyte trafficking.

Introduction

Integrins communicate signals bidirectionally across the plasma membrane and are critical for almost all migration and adhesive interactions (Shimaoka et al., 2002b). β_2 integrins are exclusively expressed on leukocytes. Integrin $\alpha_L\beta_2$ (LFA-1, leukocyte function-associated antigen-1) and the other β_2 integrins mediate leukocyte emigration from the vasculature, migration within inflammatory sites, and binding to antigen-bearing cells (Springer, 1994). The counterreceptors of $\alpha_L\beta_2$ are intercellular adhesion molecules (ICAMs) containing immunoglobulin superfamily (IgSF) domains. In contrast to $\alpha_L\beta_2$, $\alpha_M\beta_2$ (Mac-1) and $\alpha_X\beta_2$ (p150,95) recognize structurally diverse ligands, including ICAM-1, fibrinogen, and heparin sulfate. $\alpha_M\beta_2$ and $\alpha_X\beta_2$ also function as complement receptors for iC3b (CR3 and CR4, respectively).

*Correspondence: springeroffice@cbr.med.harvard.edu
[5] These authors contributed equally to this work.

Half of integrin α subunits, including all β_2 family α subunits, contain a von Willebrand factor A (VWA) or inserted (I) domain, which binds ligand at the metal ion-dependent adhesion site (MIDAS) (Shimaoka et al., 2002b). At the center of the ligand binding site, the Mg^{2+} ion held in the α_L MIDAS directly coordinates a Glu residue in ICAM-1 (Shimaoka et al., 2003b). Affinity for ligand is regulated by conformational change in the MIDAS loops, including alterations in residues that form direct coordinations. These rearrangements are communicated to the bottom face of the α I domain by a piston-like, downward movement of the C-terminal α7 helix (Shimaoka et al., 2002b). For integrins that contain α I domains, structures are available only for small ectodomain fragments (Beglova et al., 2002; Shi et al., 2005) and the α I domain itself (Lee et al., 1995; Shimaoka et al., 2003b).

Important information is lacking for integrins that contain I domains on overall ectodomain structure and how allostery is transmitted. Integrin adhesion on leukocytes is rapidly activated when engagement of other receptors on leukocytes transmits signals into the cell, which are relayed to integrin cytoplasmic and transmembrane domains. These signals are then transmitted through the ectodomain to the α I domain (Figure 1A) in a largely unknown process termed "inside-out" signaling.

In the case of integrins that lack α I domains, crystal structures, electron microscopy (EM), and small angle X-ray scattering (SAXS) have shed light on conformational motions of the ectodomain (Mould et al., 2003b; Takagi et al., 2002, 2003; Xiao et al., 2004; Xiong et al., 2001). A crystal structure of $\alpha_V\beta_3$ revealed a highly compact ectodomain, with a bend between the upper and lower α and β legs and with the ligand binding head containing the α subunit β-propeller and β I domain snuggled against the lower legs (Xiong et al., 2001). Subsequent EM structures of $\alpha_V\beta_3$ demonstrated that the bent integrin conformation is physiologic and represents a low-affinity state and that rearrangement to a state with highly extended legs occurs upon activation (Takagi et al., 2002). Moreover, two conformational states of the headpiece, termed closed and open, were observed with different angles between the β I domain and hybrid domain, and ligand binding was shown to stabilize the open conformation. An EM 3D reconstruction of the $\alpha_5\beta_1$ headpiece demonstrated that the outward swing of the hybrid domain in the open headpiece is coupled with binding to the ligand fibronectin (Takagi et al., 2003). Finally, crystal structures of the $\alpha_{IIb}\beta_3$ headpiece confirmed the EM observations on hybrid domain swing out and provided atomic views of the open, high-affinity conformation bound to ligand mimetic antagonists (Xiao et al., 2004). Rearrangements in overall ectodomain and headpiece conformations have also been supported by biochemistry, immunochemistry, and small angle X-ray scattering (Lu et al., 2001a; Luo et al., 2003; Mould et al., 2003b; Takagi et al., 2002). Nevertheless, some controversies still remain. Mechanisms for integrin activation have been proposed that do not involve leg extension or hybrid domain swing-out (Adair et al., 2005; Xiong et al., 2002).

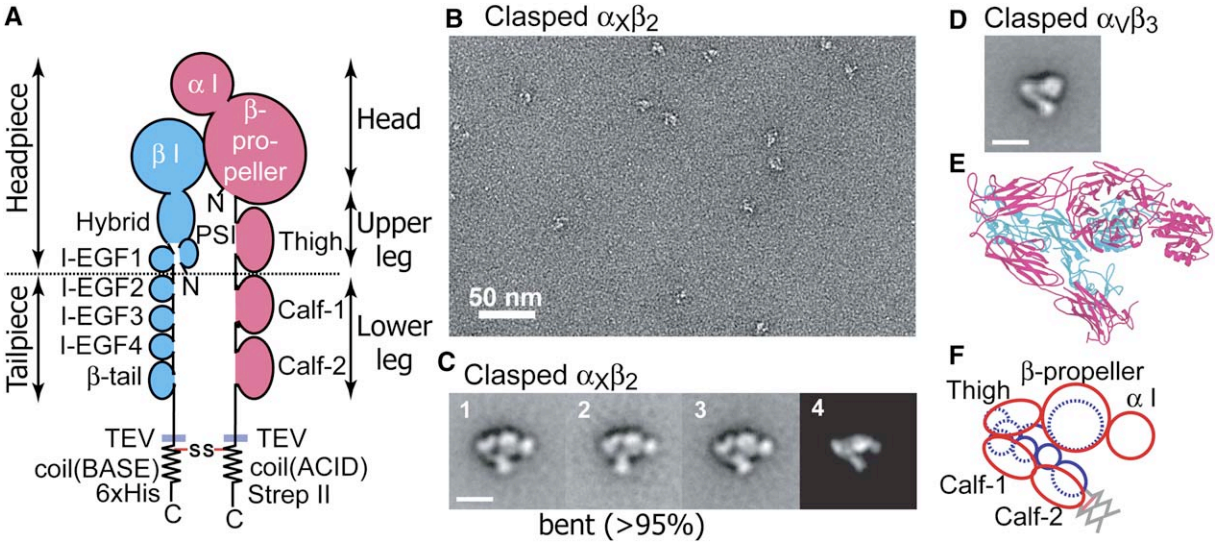

Figure 1. Clasped $\alpha_X\beta_2$ Is Bent

(A) Schematic of I domain-containing integrin ectodomain constructs.

(B) Raw image of negatively stained clasped $\alpha_X\beta_2$.

(C) The three most frequent class averages (panels 1–3) and 2D projection (panel 4) from the model of the I domain-containing integrin that correlates best to the class average in panel 1. Scale bar represents 10 nm.

(D) Representative class average of clasped $\alpha_V\beta_3$ in the bent conformation (Takagi et al., 2002). This figure is reprinted with permission of the author, Timothy A. Springer.

(E) Ribbon diagram of the pseudoatomic $\alpha_X\beta_2$ model in the same orientation as in (C), panel 4. The α and β subunits are shown in pink and cyan, respectively.

(F) A cartoon of same orientation as in (E), with the α subunit and β subunit domains outlined in red and blue, respectively. Portions of the β subunit hidden behind the α subunit are dashed.

We report here EM structures for $\alpha_L\beta_2$ and $\alpha_X\beta_2$ that address many important questions. We find that integrins that contain I domains interconvert between multiple overall ectodomain conformations. These conformations resemble those of integrins that lack I domains, despite the limited sequence identity of only 27% outside of the highly conserved α β-propeller and β I domains. We define the orientation of the α I domain relative to the β-propeller domain and find no substantial reorientation at the insertion point, as occurs upon activation at the point of insertion of the β I domain in the hybrid domain. We find that restraining integrin activation with a C-terminal clasp inhibits extension. Furthermore, one Fab fragment that is known to activate β_2 integrins on intact leukocytes induces extension, and another Fab that reports integrin activation on leukocytes binds only after induction of extension. Finally, a small-molecule allosteric antagonist induces the extended conformation with the open headpiece.

Results

Clasped $\alpha_X\beta_2$ Adopts a Bent Conformation

To obtain secreted yet physiologically relevant $\alpha_X\beta_2$ and $\alpha_L\beta_2$ ectodomains, we appended to the α and β subunits 15-residue linkers containing a TEV protease site and ACID or BASE peptides, respectively (Figure 1A; Lu et al., 2001b; Takagi et al., 2001b). The ACID and BASE peptides form a heterodimeric, disulfide-linked, α-helical coiled-coil. This coiled-coil clasp greatly augments integrin construct secretion from transfected cells (data not shown) and mimics association near the C termini of the α and β subunit extracellular domains that is mediated in intact integrins by the α and β subunit TM domains. The two linkers allow the integrin α and β subunit C termini to separate by up to 120 Å (30 residues × 4 Å/residue). Therefore, the clasp helps to stabilize, but does not dictate, α and β subunit association near their C termini. Purified protein preparations were treated as described below and subjected to gel filtration chromatography in Tris-saline containing physiologic, 1 mM concentrations of Ca^{2+} and Mg^{2+}. Samples were immediately applied to EM grids, stained with uranyl formate, and inspected by EM (see Figure S1 in the Supplemental Data available online). For each $\alpha_X\beta_2$ and $\alpha_L\beta_2$ preparation, 4000 to 9000 particles were selected and classified into 50 to 300 groups by multivariate statistical analysis and multireference alignment (Table S1). Three or more class averages are shown for each preparation, which illustrate the most populous classes, the range of conformations seen, and the most structural detail. The complete set of class averages is shown in Figure S2. Class averages were crosscorrelated with 2D projections from crystal structures resolution filtered to 25 Å, with an angular interval of 2°.

In clasped $\alpha_X\beta_2$ preparations, >95% of particles adopted compact structures (Figure 1B). Image averages reveal a homogenous bent conformation with the lower legs folding back toward the I domain-containing headpiece (Figure 1C). This conformation is quite similar to the previously described V-shaped projection structure of $\alpha_V\beta_3$ (Figure 1D; Takagi et al., 2002). The major difference is the presence of a density representing the I domain. For comparison, we used a composite atomic

model of $\alpha_X\beta_2$ (Figure 1E) constructed from the $\alpha_V\beta_3$ crystal structure (Xiong et al., 2004), additional domains that were missing in $\alpha_V\beta_3$ and were resolved in β_2 leg fragments (Beglova et al., 2002; Shi et al., 2005), and the α_X I domain crystal structure (Vorup-Jensen et al., 2003). The projection with the highest crosscorrelation coefficient (panel 4 of Figure 1C) corresponds to the orientation of the ribbon diagram of the $\alpha_X\beta_2$ model shown in Figure 1E, which is also in excellent agreement with the negative stain averages in Figure 1C. Thus, in the orientation in Figure 1C, the α_X subunit appears in front of the β_2 subunit, and the α_X I domain forms the right-most globular density (Figures 1E and 1F). Four globular densities are clearly resolved in the class averages: the head-like α_X I domain, and then counterclockwise in Figure 1C, a thorax-like density corresponding to the α_X β-propeller and β_2 I domains, a buttocks-like density corresponding to α_X and β_2 upper leg domains, and a leg-like density corresponding to α_X and β_2 lower leg domains (see Figure 1A for definition of upper and lower leg domains). The orientation of the leg-like density varies slightly in one class average compared to another (Figure 1C), demonstrating flexibility between the upper and lower legs.

Release of C-Terminal Restraints Activates $\alpha_X\beta_2$ Integrin

After the C-terminal clasp was removed by TEV protease digestion, both "compact" (bent) and "elongated" (extended) particles were observed (Figure 2A). Particle images were classified and averaged either with or without prior manual segregation into compact and elongated groups. With and without segregation, very similar percentages of particles were compact (25 and 23), extended with closed headpiece (50 and 55), and extended with open headpiece (25 and 23). However, segregation gave superior class averages for compact particles (Figure S2B). In general, manual segregation produces better results when particles adopt distinctly different sizes, because it avoids alignment of small particles with portions of large particles. The class averages of the unclasped, compact $\alpha_X\beta_2$ particles resemble the bent structure of clasped $\alpha_X\beta_2$ (Figure 2B).

In the unclasped, extended $\alpha_X\beta_2$ particles, the integrin headpiece and the extended α and β subunit legs are separately resolved. In class averages, the α subunit is shown on the right and the β subunit on the left (Figures 2C and 2D). All three α subunit leg domains (thigh, calf-1, and calf-2) were present as distinct globules in the class averages, and their orientations differed between averages (Figures 2C and 2D). The calf-1 and calf-2 domains always exhibited an extended orientation relative to one another. By contrast, there was marked flexibility of up to 130° at the genu, between the thigh and calf-1 domains (Figure 2C, compare panels 3 and 6). In the β-leg, two globular densities were observed representing the hybrid and PSI+EGF-1 domains. The remaining β-leg domains were missing in almost all class averages, suggesting substantial flexibility.

Unclasped, extended $\alpha_X\beta_2$ showed two headpiece conformations. A closed headpiece with an acute angle between the β I domain and hybrid domain was found for 50% of the particles (Figure 2C). An open headpiece with the hybrid domain swung out away from the α subunit was found in 25% of the particles (Figure 2D). The angle between the β I and hybrid domains in the closed $\alpha_X\beta_2$ headpiece was very similar to that previously observed for the closed headpiece conformation of $\alpha_V\beta_3$ (Figure 2C compared to Figure 2E, panel 1). Conversely, the angle between the β I and hybrid domains in the open headpiece conformation of $\alpha_X\beta_2$ was very similar to that previously observed in the open headpiece conformation of $\alpha_V\beta_3$ (Figure 2D compared to Figure 2E, panel 2). Importantly, there are no noticeable changes in the position of the α I domain relative to the β-propeller and β I domains between the closed and open extended conformations (Figures 2C and 2D).

Crosscorrelation was used to compare the $\alpha_X\beta_2$ averages to atomic models of the integrin headpiece. The closed headpiece structure was from the bent crystal structure model described above, whereas the open structure utilized the crystal structure of the open, high-affinity conformation of the $\alpha_{IIb}\beta_3$ headpiece, which has a distinctive angle between the β I domain and the hybrid domain (Xiao et al., 2004). The flexible lower legs were deleted from atomic models (Figures 2F and 2G, panel 3) and masked out from EM projections (Figures 2F and 2G, panel 1). The closed headpiece EM projection structure (Figure 2F, panel 1) gave an excellent crosscorrelation with projections from the closed crystal structure headpiece (Figure 2F, panel 2). The highest crosscorrelation coefficient (CCC) with closed headpiece projections of 0.79 (lowest 0.55) was much higher than the highest CCC of 0.73 (lowest 0.53) with open headpiece projections. Conversely, the open headpiece EM projection structure (Figure 2G, panel 1) crosscorrelated well with open headpiece crystal structure projections (Figure 2G, panel 2). The highest CCC with the open headpiece projections of 0.81 (lowest 0.5) was much higher than the highest CCC of 0.69 (lowest 0.53) with closed headpiece projections. These comparisons demonstrate that the two conformational states of the $\alpha_X\beta_2$ headpiece seen here in EM closely match the closed and open states of the $\alpha_V\beta_3$ and $\alpha_{IIb}\beta_3$ headpieces seen in crystal structures. In sum, our observations demonstrate that $\alpha_X\beta_2$ integrin adopts the same overall three conformational states (termed bent; extended, closed; and extended, open) that were previously observed for the $\alpha_V\beta_3$ integrin that lacks an I domain.

$\alpha_L\beta_2$ Adopts the Same Three Conformational States

For comparison, we examined the $\alpha_L\beta_2$ ectodomain via the same clasped construct design. The $\alpha_L\beta_2$ particles were more heterogeneous than for $\alpha_X\beta_2$, and clasped preparations contained both bent and extended particles (Table S1, Figures S1C and S2C). The 55% of particles categorized as compact predominantly had the same orientation on the carbon support as $\alpha_X\beta_2$ and produced class averages with a bent conformation (Figure 3A); however, in contrast to $\alpha_X\beta_2$, a range of other orientations were also observed (Figure S2C). Almost all class averages from the elongated group comprising 45% of total particles showed extended conformations (Figure 3B). Again, a wider range of orientations on the grid were observed than for $\alpha_X\beta_2$, with a few class averages appearing to represent a side orientation (Figure 3B, panel 3). Notably, the headpiece is closed in class averages of clasped, extended $\alpha_L\beta_2$ (Figure 3B), although it is possible that one or two of the 100 elongated

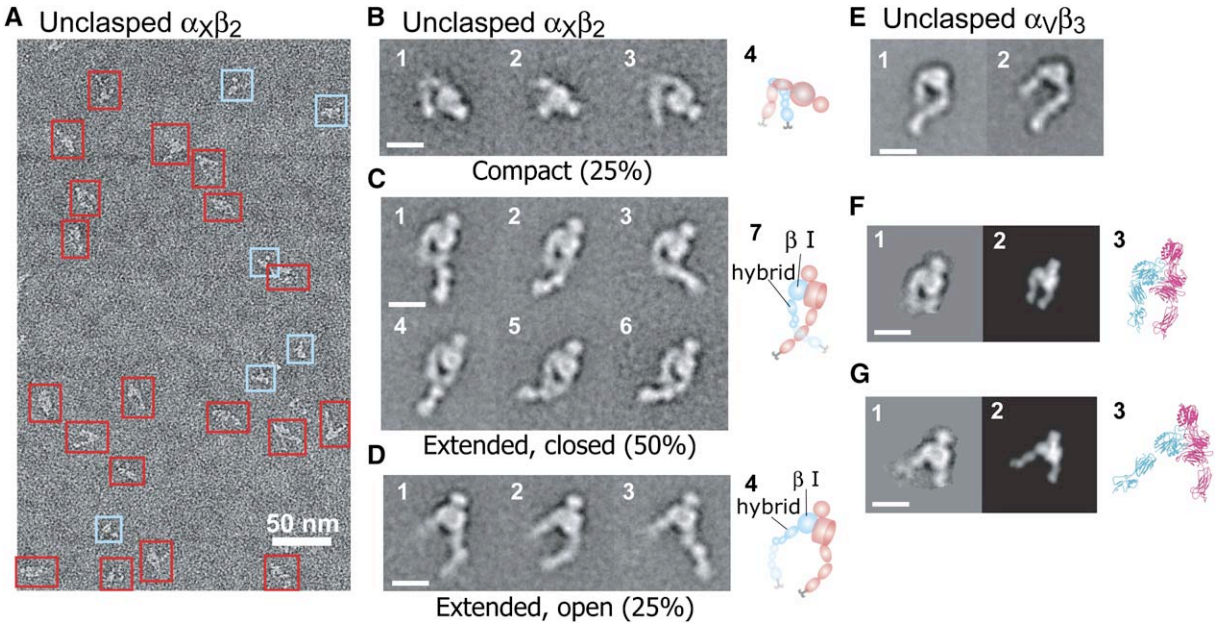

Figure 2. Unclasped $\alpha_X\beta_2$ Is Present in Multiple Conformational States

(A) Representative raw EM image of unclasped $\alpha_X\beta_2$. Particles that were segregated into compact and elongated groups are outlined with cyan and red boxes, respectively.

(B) Three representative class averages of compact group (panels 1–3) and a cartoon of the domain arrangements with α and β in red and cyan, respectively (panel 4).

(C) Six representative class averages of the elongated group with the closed headpiece conformation (panels 1–6) and a cartoon (panel 7) with the leg conformation shown in panels 2, 5, and 6.

(D) Three representative class averages of the elongated group with the open headpiece conformation and a cartoon (panel 4) with the leg conformation of panels 1 and 2.

(E) Representative class averages of unclasped $\alpha_V\beta_3$ in the extended conformation with closed headpiece (panel 1) and open headpiece (panels 2) in 2 mM Mn^{2+} (Takagi et al., 2002).

(F and G) Crosscorrelation of class averages with closed (F) and open (G) headpieces. Panel 1 shows the EM image used as a reference with the tailpiece masked out. Panel 2 represents the projection from the headpiece models with highest crosscorrelation with the reference. Panel 3 is the corresponding view of the pseudoatomic headpiece ribbon diagram (α in pink and β in cyan). Scale bars in (B)–(G) represent 10 nm.

particle class averages have an open headpiece (Figure S2C).

After the removal of the C-terminal clasp, a smaller fraction of 21% of the total $\alpha_L\beta_2$ particles adopted the bent conformation (Figure 3C). Of the total particles, 68% were extended with a closed headpiece and 11% were extended with an open headpiece (Figure 3D). Therefore, removal of the clasp increased the percentage of extended $\alpha_L\beta_2$ particles and increased the proportion of extended particles with an open headpiece.

Conformational Effect of the Small Molecule Antagonist XVA143

The α/β I allosteric antagonist XVA143 appears to bind, based on mutational studies, to the MIDAS of the β_2 I domain. Binding inhibits activation of the α I domain and induces exposure of activation epitopes in the β I domain and α and β subunit leg domains (Shimaoka et al., 2003a; Welzenbach et al., 2002; Xie et al., 2004). An $\alpha_X\beta_2$ construct in which the TEV site following the β_2 subunit was omitted enabled both clasped and unclasped constructs to be captured with antibody to the ACID-BASE coiled-coil in ELISA (Figure 4A). The KIM127 mAb binds to the β_2 I-EGF2 domain and is a reporter of β_2 integrin activation on intact cells (Lu et al., 2001a). The CBR LFA-1/2 mAb binds to the β_2 I-EGF3 domain and induces β_2 integrin activation on intact cells (Lu et al., 2001a; Petruzzelli et al., 1995). Clasped $\alpha_X\beta_2$ showed little KIM127 binding. Release of the C-terminal clasp enhanced KIM127 binding (Figure 4A). Addition of the activating mAb CBR LFA-1/2 and the allosteric antagonist did not further increase KIM127 binding to unclasped $\alpha_X\beta_2$. By contrast, CBR LFA-1/2 mAb and the antagonist XVA143 induced exposure of the KIM127 epitope in clasped $\alpha_X\beta_2$ to levels comparable to that seen in unclasped $\alpha_X\beta_2$ (Figure 4A). Furthermore, XVA143 treatment increased the hydrodynamic radius of clasped $\alpha_X\beta_2$ in size exclusion chromatography on Superdex S200 (Figure 4B).

EM showed that XVA143 treatment induced 40% of clasped $\alpha_X\beta_2$ particles to adopt the extended, open conformation (Figure 4C, panels 5–7). The remaining 60% of particles were bent (Figure 4C, panels 1–3), and no class averages with an extended, closed conformation were seen (Figure S2E). The mixture of the bent and extended, open conformations in XVA143-treated, clasped $\alpha_X\beta_2$ was present in a symmetric peak from gel filtration which had the same width as untreated, clasped $\alpha_X\beta_2$ (Figure 4B); therefore, the two conformational states must be in rapid equilibrium with one another (Stevens, 1989). With unclasped $\alpha_X\beta_2$, XVA143 induced the extended, open conformation in >95% of particles (Figure 4D). These results demonstrate (1) that XVA143 induces allostery at the β I: hybrid domain interface, which is

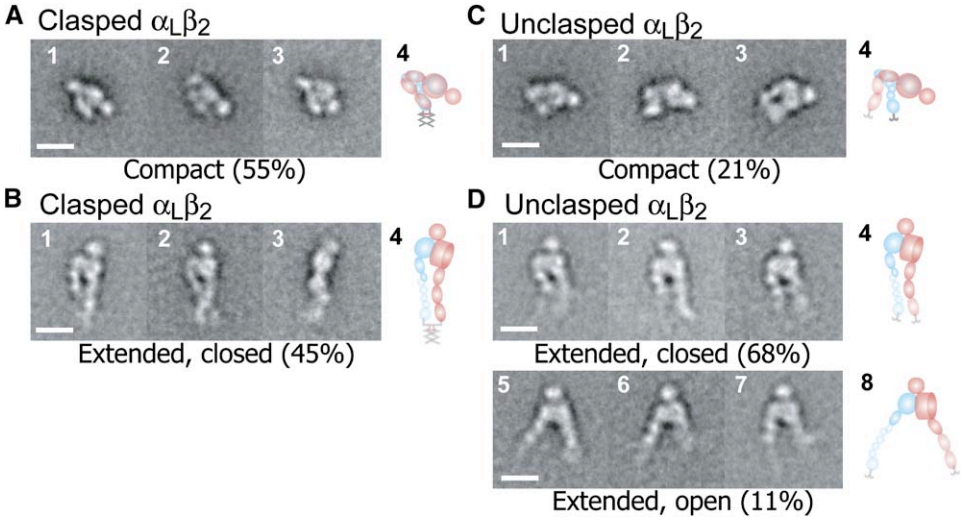

Figure 3. $\alpha_L\beta_2$ Accesses the Same Three Overall Conformational States as $\alpha_X\beta_2$

(A and B) Representative EM class averages of clasped $\alpha_L\beta_2$ obtained from the (A) compact and (B) elongated groups (panels 1–3) and a cartoon showing domain organization (panel 4, α in pink and β in cyan).

(C and D) Representative class averages of unclasped $\alpha_L\beta_2$ obtained with (C) compact and (D) elongated particles. Cartoons of representative domain organizations are shown in the rightmost panels. Scale bars represent 10 nm.

accompanied by integrin extension, and (2) that release of the C-terminal clasp lowers the energy of the extended, open conformation relative to the bent conformation.

Structural Basis for Antibody-Induced Activation

The mechanism of activation of integrins by antibodies was investigated by imaging complexes of Fab fragments with $\alpha_X\beta_2$. Complexes containing CBR LFA-1/2 Fab with clasped $\alpha_X\beta_2$ eluted markedly earlier than clasped $\alpha_X\beta_2$ alone (Figure 5A). CBR LFA-1/2 Fab induced extension of 92% of clasped $\alpha_X\beta_2$ particles (Figure 5B and Figure S1G). The remaining 8% of particles were all bent, lacked bound Fab as shown by class averages (Table S1 and Figure S2G), and are presumed to arise from Fab dissociation during gel filtration.

The bound Fab enabled observation of clearer densities for β leg domains. Approximately equal proportions of the particles adopted closed and open headpiece conformations (Figure 5B). Those with the closed headpiece conformation exhibit two different leg conformations. In leg conformation I, the α and β legs are parallel to one another, with the Fab molecule to the left of the β_2 leg (Figure 5B, panels 1–4). In leg conformation II, the β leg crosses over or under the α leg, and the Fab is to the right (Figure 5B, panels 5–8). Because of the outward swing of the hybrid domain in the open headpiece (Figure 5B, panels 9–12), in leg conformation III, the legs are more widely separated, although they bend at the genu and come closer at their C-terminal ends in order to connect at the clasp. These observations define sites of flexibility in the β_2 leg.

The class averages of CBR LFA-1/2 Fab complexes with unclasped $\alpha_X\beta_2$ were similar to those with unclasped $\alpha_X\beta_2$. Closed and open headpiece conformations were nearly equally populated (Figure 5C). Furthermore, the extended, closed complexes exhibited both parallel leg (Figure 5C, panels 1–4) and crossed leg (Figure 5C, panels 5–8) conformations.

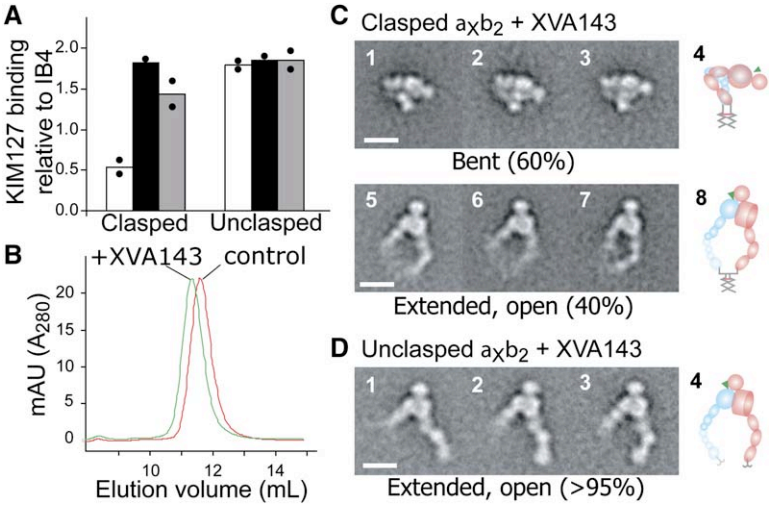

Figure 4. Conformational Rearrangements Induced by an α/β I Allosteric Antagonist

(A) ELISA measurement of KIM127 epitope expression of clasped and unclasped $\alpha_X\beta_2$ in 1 mM Ca^{2+}/Mg^{2+} (open bar), 5 μg/mL CBR LFA-1/2 antibody (black bar), and 5 μM XVA143 (gray bar). One representative experiment of three. Bars show the mean and circles show each data point of duplicates.

(B) Superdex 200 size exclusion chromatography of clasped $\alpha_X\beta_2$ in the presence and absence of XVA143.

(C and D) Representative class averages of clasped (C) and unclasped (D) $\alpha_X\beta_2$ treated with XVA143. Cartoons shown to the right of the class averages show domain arrangement and XVA143 as a green wedge at its binding site at the β I domain MIDAS (Shimaoka et al., 2003a). Scale bars represent 10 nm.

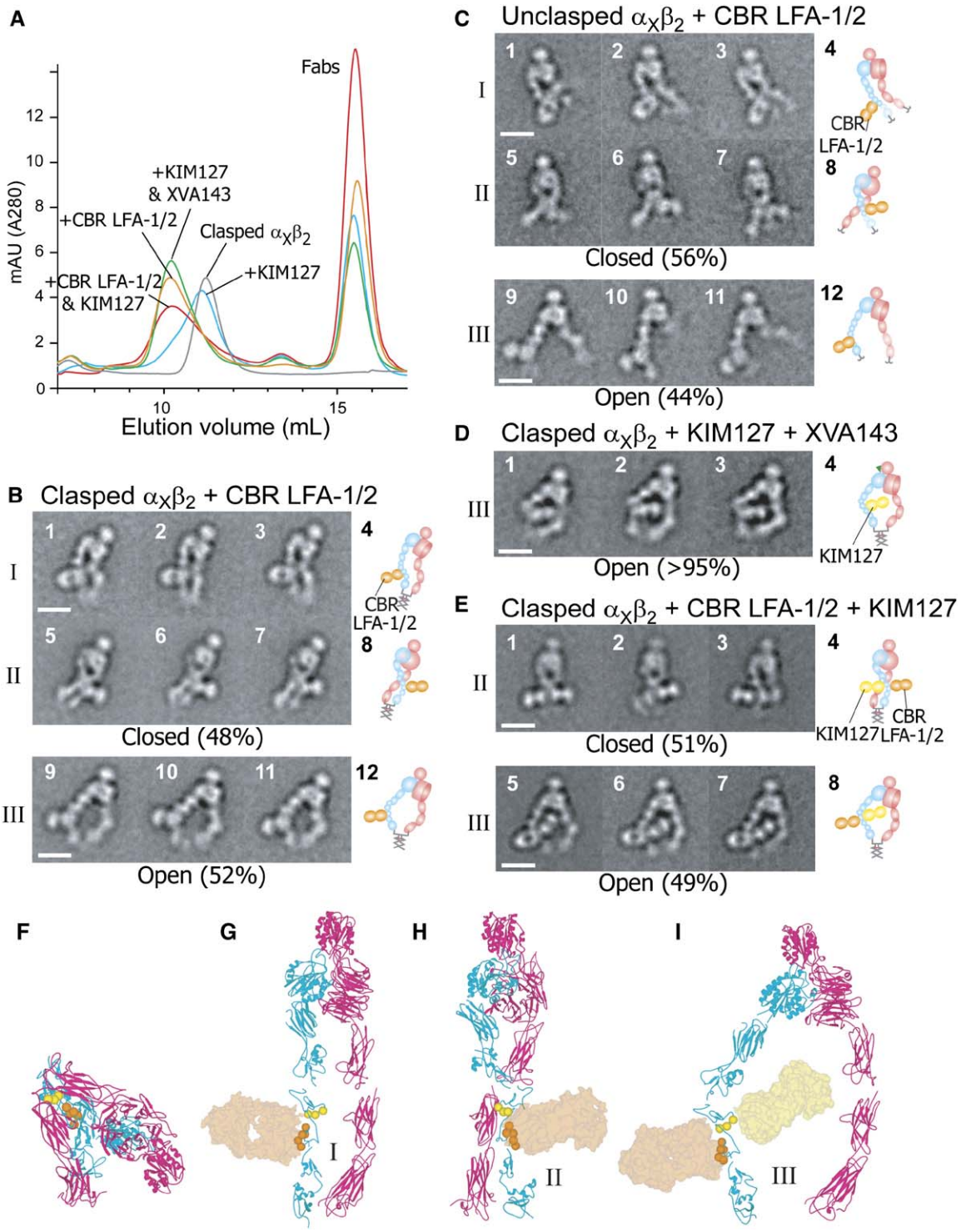

Figure 5. Induction or Reporting of Extension of $\alpha_X\beta_2$ by the CBR LFA-1/2 and KIM127 Fab

(A) Elution profiles of clasped $\alpha_X\beta_2$ in the absence and presence of Fabs in Superdex 200 size exclusion chromatography.

(B–E) Representative class averages for the indicated $\alpha_X\beta_2$, Fab, and XVA143 complexes. Designations I, II, and III refer to distinctive lower leg conformations. To the right of each set of three class averages, cartoons show domain arrangement and Fab position.

(F–I) Ribbon diagrams of pseudoatomic $\alpha_X\beta_2$ in the bent conformation (F), extended, closed conformation ([G] and [H], leg conformations I and II), and extended, open conformation ([I], leg conformation III). The α and β subunits are pink and cyan, respectively. Cα atoms of residues comprising the epitopes of CBR LFA-1/2 and KIM127 are orange and yellow spheres, respectively (Lu et al., 2001a). CBR LFA-1/2 (orange) and KIM127 (yellow) Fabs are shown as transparent surface representations. For ribbon diagrams (G)–(I), the models described in Experimental Procedures for the bent conformation and open headpiece were rotated only at the junctions between the thigh and calf-1 domains and between the I-EGF1 and 2 domains to resemble EM averages. Scale bars represent 10 nm.

Gel filtration showed only a small amount of KIM127 Fab complex formation with clasped $\alpha_X\beta_2$ (Figure 5A). By contrast, in the presence of the allosteric antagonist XVA143, complex formation with KIM127 Fab was complete (Figure 5A). A minor amount of dissociation of KIM127 Fab occurred during gel filtration. The 8% of compact particles (Table S1, Figure S1J) adopted the bent conformation with no Fab density (Figure S2J). The remaining 92% of clasped $\alpha_X\beta_2$ + KIM127 Fab + XVA143 ternary complex particles exhibited exclusively the extended, open headpiece with leg conformation III (Figure 5D). This conformation was very similar to the extended, open leg III conformation seen in the CBR LFA-1/2 complex (Figure 5B, panels 9–12); however, KIM127 bound to the opposite side of the β leg and thus occupied the space between the α and β legs (Figure 5D).

Because the CBR LFA-1/2 mAb is activating and maps to a different epitope than KIM127 (Lu et al., 2001a; Takagi et al., 2001a), we predicted that it would induce exposure of the KIM127 epitope. The complex of clasped $\alpha_X\beta_2$ with CBR LFA-1/2 Fab and KIM127 Fab (Figure 5A) was indeed ternary, with two bound Fab fragments clearly evident (Figure 5E). The open and extended, closed conformations were equally populated (Figure 5E), as seen with the CBR LFA-1/2 complex (Figure 5B). In the ternary complex with the extended, open leg III conformation (Figure 5E, panels 5–8), the KIM127 Fab binds to the inner (right) side of the β leg just as seen in the KIM127 complex in presence of XVA143 (Figure 5D), and the CBR LFA-1/2 Fab binds to the outer side of the β leg, as seen in the open CBR LFA-1/2 complex with leg III conformation (Figure 5B, panels 9–12). All CBR LFA-1/2 and KIM127 complexes with closed headpieces had the crossed leg class II conformation (Figure 5E, panels 1–4); the binding site for KIM127 Fab would appear to clash with the α leg in the parallel, class I orientation seen in Figure 5B, panels 1–4. The above results demonstrate that the CBR LFA-1/2 antibody activates integrins by inducing extension and that the KIM127 antibody reports activation because it binds only to the extended conformation.

Discussion

This study has elucidated the overall arrangement in different conformational states of the extracellular domains of two representative integrins that contain I domains and demonstrated with antibodies that extension of β_2 integrins activates ligand binding. In the resting state, $\alpha_X\beta_2$ and $\alpha_L\beta_2$ assumed a bent conformation. Crosscorrelation analysis and the presence of thorax-like, buttocks-like, and lower leg-like densities that precisely correspond to the major domains in $\alpha_V\beta_3$ strongly suggested that the shared domains are arranged very similarly in the bent conformation of $\alpha_X\beta_2$ and $\alpha_L\beta_2$, the bent $\alpha_V\beta_3$ crystal structure (Xiong et al., 2001), and the bent conformation of $\alpha_V\beta_3$ seen with negative stain EM (Takagi et al., 2002).

$\alpha_X\beta_2$ and $\alpha_L\beta_2$ were also shown to adopt extended conformations, in which the headpiece assumes one of two conformations termed closed and open. These differ in the angle between the β I domain and the β hybrid, PSI, and EGF1 domains. The hybrid and PSI/EGF-1 densities move as a rigid unit between the closed and open conformations, in agreement with crystal structure studies (Shi et al., 2005; Xiao et al., 2004). The similarity between our EM class averages and crystal structure projections showed that the angle between the β I and hybrid domains in the closed $\alpha_X\beta_2$ and $\alpha_L\beta_2$ headpieces is very similar to that in the crystal structure of the bent, closed, low-affinity $\alpha_V\beta_3$ conformation and showed that the β I-hybrid domain angle in open $\alpha_X\beta_2$ and $\alpha_L\beta_2$ is very similar to that in the crystal structure of the open, high-affinity $\alpha_{IIb}\beta_3$ conformation.

Atomic structures of β_3 integrins show that reshaping of the ligand binding site atop the β I domain is linked to a downward movement in its C-terminal α7 helix that connects to the hybrid domain at the bottom of the β I domain, causing pivoting about the other, N-terminal connection, and the observed outward swing of the hybrid domain in the open headpiece. Residues that coordinate MIDAS and ADMIDAS metal ions and hydrophobic residues in the β6-α7 loop and α1 loop that insert in alternate hydrophobic pockets act as ratchets that stabilize the open and closed conformations as discrete states (Xiao et al., 2004). We observed discrete open and closed headpiece class averages over conditions in which the relative population of the two states differed widely, without evidence for intermediate headpiece conformations. This finding in β_2 integrins suggested that two discrete states at the β I domain-hybrid domain interface is a general feature of integrin allostery.

The bent and extended structures showed that the α I domain, which is inserted in the α subunit β-propeller domain, extends away from the β-propeller near its interface with the β I domain. The I domain binds ligand at its MIDAS, which is on the face opposite to the points of insertion in the β-propeller (Lee et al., 1995; Shimaoka et al., 2002b). With the range of observed orientations of the lower legs with respect to the remainder of bent $\alpha_X\beta_2$ and with the lower leg normal to the plasma membrane, the ligand binding site of the α I domain ranges from pointing toward the membrane about 8 Å above it to pointing sideways across the membrane about 74 Å above it (Figure 6A).

Extension of β_2 integrins was found to dramatically alter the disposition of the α I domain. In extended integrins, the ligand binding face of the α I domain is oriented in the opposite direction from the legs that connect to the cell membrane (Figure 6B). Furthermore, with the legs normal to the membrane, the ligand binding face of the α I domain is 230 to 250 Å away from the cell surface, about 200 Å further away than in the bent conformation. Extension thus primes integrins with I domains for binding to ligands on other cells, the matrix, or opsonized surfaces.

Crystal structures of isolated α I domains demonstrate a 10 Å downward movement of the C-terminal α helix in the active state (Lee et al., 1995). However, in contrast to the movement at the point of β I domain insertion in the hybrid domain, we saw no similar large-scale motion at the point of insertion of the α I domain in the β-propeller domain. This is consistent with the idea that allostery is transmitted to the α I domain not through the β-propeller domain, but through the β I domain. An invariant Glu residue that follows the C-terminal α7 helix of the α I domain comes into close contact with the β I domain MIDAS in α I domain activation (Yang et al., 2004b), and binding

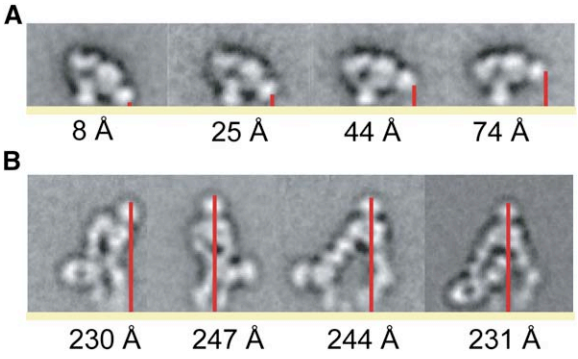

Figure 6. Disposition of the Ligand Binding Face of the α I Domain in Bent and Extended Conformations

Class averages displaying wide variation in the angle between the head and lower legs were chosen for clasped bent (A) and clasped extended (B) αXβ2 conformations and oriented with the lower legs normal to an imaginary plasma membrane. The red line shows the distance between the ligand binding site of the α_X I domain and the plasma membrane, and this distance is shown beneath each panel.

of this Glu to the activated β I MIDAS is thought to exert a pull on the α7 helix that transmits allostery to the α I MIDAS (Alonso et al., 2002; Yang et al., 2004b). Upon binding of this Glu, a relatively firm interface between the α I and β-propeller domains, as suggested by the studies here, would favor downward displacement of the α7 helix, rather than tilting of the α I domain relative to the β-propeller domain.

Our study has provided important information about the flexibility of the integrin legs. In extended $\alpha_V\beta_3$, the angle between the thigh and calf-1 domains is uniform, suggesting that the genu has a preferred conformation in the extended state (Takagi et al., 2002). By contrast, in extended $\alpha_X\beta_2$, we found that the angle at the genu can vary by up to 130°. On the other hand, the orientations between the α subunit β-propeller and thigh domains and between the calf-1 and calf-2 domains are fairly uniform and are similar in $\alpha_X\beta_2$ and $\alpha_V\beta_3$.

The KIM127 Fab, which binds to I-EGF2 (Lu et al., 2001a), flipped position between class averages in which the β leg was parallel to or crossed the α leg. Therefore, the β leg is flexible above I-EGF2. The bend in the β leg appears to occur between I-EGF domains 1 and 2 (Takagi et al., 2002). Our findings demonstrated marked flexibility of the integrin leg at this interface. Additional flexibility was seen between lower β leg domains; however, most of the differences seen between leg conformations I, II, and III are attributable to motions between I-EGF1 and I-EGF2 in β and between thigh and calf-1 in α.

Our studies have provided insights into how signals are transmitted between domains in integrins and how this regulates the relative stabilities of the bent; extended, closed; and extended, open conformational states. Mutational and fluorescent resonance energy transfer (FRET) studies on β_2 and β_3 integrins in intact cells show that close association between the cytoplasmic and transmembrane domains maintains the resting, low-affinity state and that integrin activation is closely associated with their separation (Kim et al., 2003; Lu et al., 2001b; Luo et al., 2004a). We used a C-terminal covalent clasp to mimic association of the α and β subunit transmembrane and cytoplasmic domains. In the presence of the clasp, almost all $\alpha_X\beta_2$ particles and the majority of the $\alpha_L\beta_2$ particles were in the bent conformation. By contrast, after clasp removal, more than 75% of $\alpha_X\beta_2$ and $\alpha_L\beta_2$ particles adopted extended conformations. Our results with soluble constructs supported the conclusion that on the cell surface, association of the integrin α and β subunit transmembrane domains stabilizes the bent conformation of the ectodomain.

Physiologic studies of β_2 integrins on intact cells show that CBR LFA-1/2 mAb induces the high-affinity state and that KIM127 mAb can either stabilize or report the high-affinity state (Andrew et al., 1993; Evangelista et al., 1996; Kim et al., 2003, 2004; Lu et al., 2001a; Petruzzelli et al., 1995; Robinson et al., 1992; Salas et al., 2004; Shimaoka et al., 2002a; Takami et al., 2001; Yang et al., 2004b). The binding sites for KIM127 and CBR LFA-1/2 antibodies map to specific mouse-human amino acid substitutions in the I-EGF2 and I-EGF3 domains, respectively (Lu et al., 2001a; Takagi et al., 2001a). An NMR structure for β_2 I-EGF3 and NOE constraints between I-EGF domains 2 and 3 define the orientation between domain 3 and a homology model of domain 2 (Beglova et al., 2002). The KIM127 and CBR LFA-1/2 epitopes locate on opposite faces of this NMR/homology model (Beglova et al., 2002), in excellent agreement with our finding here that KIM127 and CBR LFA-1/2 Fab bound to opposite sides of the β_2 leg. The current study has definitively established that the CBR LFA-1/2 and KIM127 antibodies induce or report the active integrin state by binding to the extended conformation. We examined a total of 840 class averages of clasped $\alpha_X\beta_2$ + CBR LFA-1/2 Fab, clasped $\alpha_X\beta_2$ + CBR LFA-1/2 Fab + KIM127 Fab, clasped $\alpha_X\beta_2$ + XVA143 + KIM127 Fab, and unclasped $\alpha_X\beta_2$ + CBR LFA-1/2 Fab. Not a single one of these class averages showed a bent integrin bound to Fab. Although clasped $\alpha_X\beta_2$ was >95% bent in the absence of Fab, we found Fab bound only to the extended conformation.

Because of the wide range of studies cited above with antibodies to these epitopes on intact cells, the current EM studies on $\alpha_X\beta_2$ Fab complexes have definitively established that extension is sufficient to activate ligand binding competence by β_2 integrins (Evangelista et al., 1996; Kim et al., 2003, 2004; Lu et al., 2001a; Petruzzelli et al., 1995; Shimaoka et al., 2002a; Takami et al., 2001; Yang et al., 2004a, 2004b); that ligand-bound β_2 integrins on cell surfaces are extended (Andrew et al., 1993; Robinson et al., 1992); that binding to soluble ligand induces extension (Salas et al., 2004); and finally, that extracellular activation of integrins by Mn^{2+} as well as inside-out activation of integrins stimulated by protein kinase C, or activating cytoplasmic domain mutations, induces the extended conformation in the absence of ligand binding (Kim et al., 2003, 2004; Lu et al., 2001a).

Our study defined the interrelationship between two key conformational transitions in integrins, leg extension and the outward swing of the hybrid domain. C-terminal separation (unclasping) of $\alpha_X\beta_2$ and $\alpha_L\beta_2$, and activating Fab, induced extended conformations in which the open and closed headpieces were similarly populated. Therefore, C-terminal separation and the CBR LFA-1/2 Fab activate by inducing extension, which in turn enables, but does not enforce, a second conformational

transition to the open headpiece, the putative high-affinity form. The $\alpha_X\beta_2$ and $\alpha_L\beta_2$ integrins appear to have distinct setpoints for these transitions. Clasped $\alpha_X\beta_2$ was more stable in the bent conformation than $\alpha_L\beta_2$, whereas when extended, a higher proportion $\alpha_X\beta_2$ than $\alpha_L\beta_2$ assumed the open, putative high-affinity conformation. Interfaces between the α_X and β_2 subunits in the bent conformation regulate the energetics of activation (Beglova et al., 2002; Zang and Springer, 2001). The greater propensity of $\alpha_L\beta_2$ to extend found here is in agreement with the greater exposure of β leg activation epitopes by $\alpha_L\beta_2$ than $\alpha_X\beta_2$ on the surface of unstimulated cells (Lu et al., 2001a). Furthermore, extension of $\alpha_L\beta_2$ is functionally important for its ability to support transient adhesive interactions including rolling in shear flow (Salas et al., 2002, 2004).

The allosteric antagonist XVA143 was found to act at the step of headpiece opening rather than extension, because it induced exclusively extended molecules with open headpieces. The linkage between the equilibria for extension and headpiece opening was clearly demonstrated by the finding that clasped $\alpha_X\beta_2$, which is >95% bent, was converted only 40% to extended, open molecules by XVA143, whereas unclasped $\alpha_X\beta_2$, which is predominantly extended, was converted essentially 100% by XVA143 to extended, open molecules. Bent molecules with open headpieces were not seen and therefore must be unstable. This is in agreement with an analysis of the bent $\alpha_V\beta_3$ structure, which shows that the hybrid domain is the most buried of all domains in α leg-β leg and headpiece-tailpiece interfaces (Takagi et al., 2002). The extensive disruption of interfaces by hybrid domain swing-out explains the linkage between allosteric antagonist-induced headpiece opening and integrin extension.

Previous studies show that allosteric α/β I antagonists greatly enhance $\alpha_L\beta_2$-dependent leukocyte rolling adhesion in vitro on ICAM-1 substrates and in vivo on high endothelial venules and block $\alpha_L\beta_2$-dependent firm adhesion (Salas et al., 2004). Rolling adhesion and firm adhesion are mediated by α I domains with low and high affinity, respectively (Salas et al., 2002). The marked enhancement by the allosteric antagonist of rolling adhesion was explained here by the more exposed orientation of the α_L I domain and its ~200 Å increase in height above the membrane in the extended compared to the bent conformation.

EM and crystallography show that hybrid domain swing-out is induced in the $\alpha_V\beta_3$ and $\alpha_{IIb}\beta_3$ integrins by Arg-Gly-Asp (RGD) ligand mimetics (Takagi et al., 2002; Xiao et al., 2004) and in integrin $\alpha_5\beta_1$ by RGD peptide and fibronectin fragments (Takagi et al., 2003). The similar ability of the β_2 integrin allosteric antagonist to induce hybrid domain swing-out observed here agrees with a previous conclusion that α/β I allosteric antagonists and α/β I competitive antagonists, such as Arg-Gly-Asp ligand mimetics, have similar binding sites and allosteric effects (Shimaoka et al., 2003a).

Our study has revealed that two integrins that contain I domains, $\alpha_X\beta_2$ and $\alpha_L\beta_2$, transition between bent, extended, closed, and extended, open conformations. Although one recent study failed to observe $\alpha_V\beta_3$ extension (Adair et al., 2005), the extended integrin conformation has been widely observed by EM for many years, including for $\alpha_5\beta_1$ (Nermut et al., 1988; Takagi et al., 2001b) and $\alpha_{IIb}\beta_3$ bound to its ligand fibrinogen (Du et al., 1993). Furthermore, hybrid domain swing-out or its role in activation of the high-affinity state has now been observed in five different integrins: $\alpha_V\beta_3$ (Luo et al., 2003; Takagi et al., 2002), $\alpha_{IIb}\beta_3$ (Luo et al., 2003, 2004c; Mould et al., 2003a; Xiao et al., 2004), $\alpha_5\beta_1$ (Luo et al., 2004b; Mould et al., 2003b; Takagi et al., 2003), $\alpha_L\beta_2$, and $\alpha_X\beta_2$. Thus, structural and functional similarities have been seen among distantly related members of the integrin family. Furthermore, the studies here with CBR LFA-1/2 and KIM127 Fab have demonstrated that extension is sufficient to induce activation and that activation of the high-affinity state on the cell surface is associated with extension. Our studies thus explain at the molecular level how immunologically important integrins become activated in the immunological synapse in immune responses, at the leukocyte-endothelial interface in leukocyte trafficking from blood to tissues, and in phagocytosis of opsonized pathogens.

Experimental Procedures

Protein Preparation

Soluble, heterodimeric $\alpha_L\beta_2$ and $\alpha_X\beta_2$ constructs were prepared from wild-type human α_L, α_X, and β_2 cDNAs by PCR and standard molecular cloning techniques. In brief, α subunit cDNAs, encoding the signal sequence and mature residues 1–1063 of α_L or 1–1084 of α_X, were fused to a C-terminal 53-residue peptide, GTGG**LENLYFQG** GEN<u>AQCEKELQALEKENAQLEWELQALEKELAQ</u>*WSHPQFEK* containing a TEV protease recognition site (bold), an acidic coiled-coil region and a cysteine for disulfide bond formation (underlined) (Takagi et al., 2001b), and a Strep-II tag (italics) by PCR and incorporated into the XbaI and HindIII sites of the pcDNA3.1/Hygro(-) expression vector (Invitrogen, Carlsbad, CA). Similarly, a cDNA encoding the signal sequence and mature residues 1–677 of β_2 was inserted into the NotI and PmeI sites of the pEF1-puro vector (Takagi et al., 2001b), with a C-terminal sequence DTSG**LENLYFQG** GKN<u>AQCKKKLQALKKKNAQLKWKLQALKKKLAQ</u>GG*HHHHHH* containing a TEV protease recognition site (bold), a basic coiled-coiled region with a cysteine (underlined) (Takagi et al., 2001b), and a hexahistidine tag (italics). CHO Lec 3.2.8.1 cells were cotransfected with these vectors by electroporation and selected in 10 μg/ml puromycin and 400 μg/ml hygromycin-B and screened for secretion of soluble integrin by sandwich ELISA via a capture antibody to the coiled-coil (Takagi et al., 2001b) and biotinylated detection mAb IB4 to β_2. The clone with the highest secretion level was cultured in the medium described in Casasnovas and Springer (1995) supplemented with 5% FCS, 10 μg/ml puromycin, and 400 μg/ml hygromycin-B in roller bottles at 37°C, and culture supernatants were harvested every week. Soluble integrins were purified from the culture supernatant by a Ni-NTA affinity chromatography (QIAGEN, Valencia, CA) followed by application to a Strep-Tactin column (IBA). To obtain unclasped integrins, purified clasped integrins (1 mg/ml) were treated with recombinant His-tagged TEV protease (Invitrogen) at 250 U/mg integrin at room temperature for 16 hr, followed by re-pass-through the Ni-NTA column. The flow-through containing purified unclasped integrins was dialyzed against and stored in TBS/Ca/Mg buffer (20 mM Tris-HCl [pH 7.5], 150 mM NaCl, 1 mM $CaCl_2$, 1 mM $MgCl_2$). For ELISA experiments, the TEV protease recognition sequence of the β_2 subunit was abolished by mutation of ENLYF**QG** to ENLYFHS with Quikchange (Stratagene, La Jolla, CA). HEK293S GNTI-negative cells (Reeves et al., 2002) were transfected by calcium phosphate (Lu et al., 2001a) and cultured for 6 days after transfection. Protein was purified from culture supernatant as described above.

The murine mAbs CBR-LFA1/2 (Petruzzelli et al., 1995) and KIM127 (Robinson et al., 1992) to human β_2 have been described. IgG was purified with a protein A column. Fab fragments were

prepared with bead-immobilized papain according to the manufacturer's instruction (Pierce Chemical Co., Rockford, IL), followed by re-pass-through the protein A column to remove undigested IgG and Fc fragment. XVA143 was a generous gift from Dr. Paul Gillespie (Hoffman LaRoche, Nutley, NJ) (Welzenbach et al., 2002).

Grid Preparation, Electron Microscopy, and Image Processing

$\alpha_X\beta_2$ (0.1 ml of 0.2 to 0.5 mg/ml) was subjected to Superdex 200 (Amersham Biosciences, Piscataway, NJ) gel permeation chromatography in TBS/Ca/Mg buffer. For XVA143, $\alpha_X\beta_2$ in 10 μM XVA143 was injected in a column equilibrated with TBS/Ca/Mg and 1 μM XVA143. For Fab complexes, approximately 0.2 mg/mL clasped and unclasped $\alpha_X\beta_2$ integrins were incubated at room temperature for 15 min with a 6 molar excess (0.25 mg/mL) of each Fab. The complex of clasped $\alpha_X\beta_2$ and KIM127 Fab was formed in the presence of 50 μM XVA143 and subjected to gel filtration in TBS/Ca/Mg, and fractions were immediately supplemented with 10 μM XVA143. Gel permeation chromatography of $\alpha_L\beta_2$ was in 25 mM MES (pH 6.0), 150 mM NaCl, 5 mM $CaCl_2$, which yielded better staining than at pH 7.5. Peak fractions were diluted to 1–5 μg/mL and applied to grids within 10 to 120 min after elution. Preparation of negatively stained samples, acquisition of micrographs, and image digitization were as described (Takagi et al., 2002).

Image processing was performed with SPIDER, via the multireference alignment procedure described at http://www.wadsworth.org/spider_doc/spider/docs/align.html and the associated graphical user interface WEB (Frank et al., 1996). 4000–9000 particles were picked interactively, windowed into 100 × 100 pixel images (4.04 Å/pixel), and centered. Images were rotationally and translationally aligned by a multireference alignment procedure and subjected to K-means classification specifying between 20 and 300 classes depending on the structural heterogeneity of the particle population (Table S1). This alignment and classification procedure was iterated 10 times to obtain the final class averages. For clasped and unclasped $\alpha_L\beta_2$ and unclasped $\alpha_X\beta_2$, particles in the same set of images were segregated into compact and elongated groups; i.e., the number of particles in each group reflected their abundance on the grids. Each group was independently subjected to alignment and classification. For integrin-Fab complexes, extended particles (92% for the clasped $\alpha_X\beta_2$ + CBR LFA-1/2 and the clasped $\alpha_X\beta_2$ + KIM127 + XVA143 complexes and >95% for all other complexes) were subjected to image averaging. As a control, all particles in clasped $\alpha_X\beta_2$ + CBR LFA-1/2 and clasped $\alpha_X\beta_2$ KIM127 + XVA143 preparations that were excluded by the above criteria (i.e., the compact particles) were separately subjected to image averaging to test whether Fab could bind to bent particles (Table S1). To calculate the percentage of particles that were bent, extended, open, or extended, closed, all class averages were categorized, and the number of particles in these averages was summed and divided by the total number of particles. This total number included particles segregated into compact and elongated groups.

Crosscorrelation was as described (Takagi et al., 2002). Projections from 25 Å resolution-filtered 3D maps were aligned with the reference EM image both translationally and rotationally by means of an appropriately sized circular mask (35 and 30 pixels in radius for headpiece and bent models, respectively). The crosscorrelation coefficient was normalized by dividing by the maximum correlation coefficient between a pair of EM images.

Atomic Models of the Ectodomain and Headpiece

Pseudoatomic models of I domain-containing integrin ectodomains were built starting with the coordinates of $\alpha_V\beta_3$ (PDB entry 1U8C). To add I-EGF1, a β_2 hybrid-PSI-EGF1 domain fragment (PDB entry 1YUK) was superimposed with the hybrid and PSI domains, and the β_2 hybrid and PSI domains were used to replace those of β_3. The I-EGF2 domain was added and the I-EGF3 domain of β_3 was replaced by that of β_2 after superposition with I-EGF3 of the NMR-based model of β_2 I-EGF domains 2 and 3 (Beglova et al., 2002). The crystal structure of the α_X I domain (PDB entry 1N3Y) was positioned so that its C and N termini were near the insertion point in the β-propeller and its C terminus was near the β I MIDAS. The closed headpiece model was obtained by omitting the calf-1, calf-2, I-EGF2, 3, and 4, and β-tail domains. The open headpiece model was obtained by superimposing domains of the closed headpiece model on the crystal coordinates of the liganded-open activated $\alpha_{IIb}\beta_3$ headpiece (PDB entry 1TXV) (Xiao et al., 2004).

Integrin structures in the extended conformations were modeled by rigid body movements of the lower legs relative to the closed and open headpieces at the α genu and the β I-EGF-1 and 2 junction. The orientations of the lower legs were adjusted to resemble EM averages of clasped $\alpha_X\beta_2$ in complex with mAbs (Figures 5G–5I). Fabs in the model structures were from crystal coordinates of 10E5 Fab in $\alpha_{IIb}\beta_3$ headpiece structure (Xiao et al., 2004). Models were built by UCSF Chimera (Pettersen et al., 2004).

ELISA

Microtiter wells were coated overnight at 4°C with 50 μl of 5 μg/ml rabbit polyclonal anti-velcro antibody (Takagi et al., 2001b) and blocked with 1% (w/v) bovine serum albumin. Clasped or unclasped $\alpha_X\beta_2$ (50 μl, 0.5 μg/ml) were incubated for 2 hr at room temperature. After three washes, wells were incubated with or without 5 μg/ml mAb CBR LFA1/2, or 5 μM XVA143 in TBS/Ca/Mg at room temperature for 15 min, and then incubated in the presence of 1 μg/ml of biotinylated KIM127 or IB_4 mAb (Ancell Corporation, Bayport, MN) for another 15 min at room temperature. Antibody binding was detected by streptavidin-labeled HRP (Invitrogen) and substrate (Zymed, San Francisco, CA).

Supplemental Data

Supplemental Data include three figures and one table and can be found with this article online at http://www.immunity.com/cgi/content/full/25/4/583/DC1/.

Acknowledgments

This work was supported by NIH grants AI72765 (T.A.S.), AI63421 (M.S.), and GM62580 (T.W.) and the Astellas Foundation for Research on Metabolic Disorders and Yoshida Scholarship Foundation (N.N.). We thank Dr. T. Nakagawa for help with the EM experiments.

Received: June 1, 2006
Revised: July 26, 2006
Accepted: July 26, 2006
Published online: October 12, 2006

References

Adair, B.D., Xiong, J.P., Maddock, C., Goodman, S.L., Arnaout, M.A., and Yeager, M. (2005). Three-dimensional EM structure of the ectodomain of integrin αVβ3 in a complex with fibronectin. J. Cell Biol. *168*, 1109–1118.

Alonso, J.L., Essafi, M., Xiong, J.P., Stehle, T., and Arnaout, M.A. (2002). Does the integrin αA domain act as a ligand for its βA domain? Curr. Biol. *12*, R340–R342.

Andrew, D., Shock, A., Ball, E., Ortlepp, S., Bell, J., and Robinson, M. (1993). KIM185, a monoclonal antibody to CD18 which induces a change in the conformation of CD18 and promotes both LFA-1- and CR3-dependent adhesion. Eur. J. Immunol. *23*, 2217–2222.

Beglova, N., Blacklow, S.C., Takagi, J., and Springer, T.A. (2002). Cysteine-rich module structure reveals a fulcrum for integrin rearrangement upon activation. Nat. Struct. Biol. *9*, 282–287.

Casasnovas, J.M., and Springer, T.A. (1995). Kinetics and thermodynamics of virus binding to receptor: studies with rhinovirus, intercellular adhesion molecule-1 (ICAM-1), and surface plasmon resonance. J. Biol. Chem. *270*, 13216–13224.

Du, X., Gu, M., Weisel, J.W., Nagaswami, C., Bennett, J.S., Bowditch, R., and Ginsberg, M.H. (1993). Long range propagation of conformational changes in integrin $\alpha_{IIb}\beta_3$. J. Biol. Chem. *268*, 23087–23092.

Evangelista, V., Manarini, S., Rotondo, S., Martelli, N., Polischuk, R., McGregor, J.L., de Gaetano, G., and Cerletti, C. (1996). Platelet/polymorphonuclear leukocyte interaction in dynamic conditions: evidence of adhesion cascade and cross talk between P-selectin and the β2 integrin CD11b/CD18. Blood *88*, 4183–4194.

Frank, J., Radermacher, M., Penczek, P., Zhu, J., Li, Y., Ladjadj, M., and Leith, A. (1996). SPIDER and WEB: processing and visualization of images in 3D electron microscopy and related fields. J. Struct. Biol. *116*, 190–199.

Kim, M., Carman, C.V., and Springer, T.A. (2003). Bidirectional transmembrane signaling by cytoplasmic domain separation in integrins. Science *301*, 1720–1725.

Kim, M., Carman, C.V., Yang, W., Salas, A., and Springer, T.A. (2004). The primacy of affinity over clustering in regulation of adhesiveness of the integrin αLβ2. J. Cell Biol. *167*, 1241–1253.

Lee, J.-O., Rieu, P., Arnaout, M.A., and Liddington, R. (1995). Crystal structure of the A domain from the α subunit of integrin CR3 (CD11b/CD18). Cell *80*, 631–638.

Lu, C., Ferzly, M., Takagi, J., and Springer, T.A. (2001a). Epitope mapping of antibodies to the C-terminal region of the integrin β2 subunit reveals regions that become exposed upon receptor activation. J. Immunol. *166*, 5629–5637.

Lu, C., Takagi, J., and Springer, T.A. (2001b). Association of the membrane-proximal regions of the α and β subunit cytoplasmic domains constrains an integrin in the inactive state. J. Biol. Chem. *276*, 14642–14648.

Luo, B.-H., Springer, T.A., and Takagi, J. (2003). Stabilizing the open conformation of the integrin headpiece with a glycan wedge increases affinity for ligand. Proc. Natl. Acad. Sci. USA *100*, 2403–2408.

Luo, B.-H., Springer, T.A., and Takagi, J. (2004a). A specific interface between integrin transmembrane helices and affinity for ligand. PLoS Biol. *2*, 776–786.

Luo, B.-H., Strokovich, K., Walz, T., Springer, T.A., and Takagi, J. (2004b). Allosteric β1 integrin antibodies that stabilize the low affinity state by preventing the swing-out of the hybrid domain. J. Biol. Chem. *279*, 27466–27471.

Luo, B.-H., Takagi, J., and Springer, T.A. (2004c). Locking the β3 integrin I-like domain into high and low affinity conformations with disulfides. J. Biol. Chem. *279*, 10215–10221.

Mould, A.P., Barton, S.J., Askari, J.A., McEwan, P.A., Buckley, P.A., Craig, S.E., and Humphries, M.J. (2003a). Conformational changes in the integrin βA domain provide a mechanism for signal transduction via hybrid domain movement. J. Biol. Chem. *278*, 17028–17035.

Mould, A.P., Symonds, E.J., Buckley, P.A., Grossmann, J.G., McEwan, P.A., Barton, S.J., Askari, J.A., Craig, S.E., Bella, J., and Humphries, M.J. (2003b). Structure of an integrin-ligand complex deduced from solution X-ray scattering and site-directed mutagenesis. J. Biol. Chem. *278*, 39993–39999.

Nermut, M.V., Green, N.M., Eason, P., Yamada, S.S., and Yamada, K.M. (1988). Electron microscopy and structural model of human fibronectin receptor. EMBO J. *7*, 4093–4099.

Petruzzelli, L., Maduzia, L., and Springer, T.A. (1995). Activation of LFA-1 (CD11a/CD18) and Mac-1 (CD11b/CD18) mimicked by an antibody directed against CD18. J. Immunol. *155*, 854–866.

Pettersen, E.F., Goddard, T.D., Huang, C.C., Couch, G.S., Greenblatt, D.M., Meng, E.C., and Ferrin, T.E. (2004). UCSF Chimera—a visualization system for exploratory research and analysis. J. Comput. Chem. *25*, 1605–1612.

Reeves, P.J., Callewaert, N., Contreras, R., and Khorana, H.G. (2002). Structure and function in rhodopsin: high-level expression of rhodopsin with restricted and homogeneous N-glycosylation by a tetracycline-inducible N-acetylglucosaminyltransferase I-negative HEK293S stable mammalian cell line. Proc. Natl. Acad. Sci. USA *99*, 13419–13424.

Robinson, M.K., Andrew, D., Rosen, H., Brown, D., Ortlepp, S., Stephens, P., and Butcher, E.C. (1992). Antibody against the Leu-cam β-chain (CD18) promotes both LFA-1-and CR3-dependent adhesion events. J. Immunol. *148*, 1080–1085.

Salas, A., Shimaoka, M., Chen, S., Carman, C.V., and Springer, T.A. (2002). Transition from rolling to firm adhesion is regulated by the conformation of the I domain of the integrin LFA-1. J. Biochem. (Tokyo) *277*, 50255–50262.

Salas, A., Shimaoka, M., Kogan, A.N., Harwood, C., von Andrian, U.H., and Springer, T.A. (2004). Rolling adhesion through an extended conformation of integrin αLβ2 and relation to α I and β I-like domain interaction. Immunity *20*, 393–406.

Shi, M., Sundramurthy, K., Liu, B., Tan, S.M., Law, S.K., and Lescar, J. (2005). The crystal structure of the plexin-semaphorin-integrin domain/hybrid domain/I-EGF1 segment from the human integrin β2 subunit at 1.8-A resolution. J. Biol. Chem. *280*, 30586–30593.

Shimaoka, M., Lu, C., Salas, A., Xiao, T., Takagi, J., and Springer, T.A. (2002a). Stabilizing the integrin αM inserted domain in alternative conformations with a range of engineered disulfide bonds. Proc. Natl. Acad. Sci. USA *99*, 16737–16741.

Shimaoka, M., Takagi, J., and Springer, T.A. (2002b). Conformational regulation of integrin structure and function. Annu. Rev. Biophys. Biomol. Struct. *31*, 485–516.

Shimaoka, M., Salas, A., Yang, W., Weitz-Schmidt, G., and Springer, T.A. (2003a). Small molecule integrin antagonists that bind to the β2 subunit I-like domain and activate signals in one direction and block them in another. Immunity *19*, 391–402.

Shimaoka, M., Xiao, T., Liu, J.-H., Yang, Y., Dong, Y., Jun, C.-D., McCormack, A., Zhang, R., Joachimiak, A., Takagi, J., et al. (2003b). Structures of the αL I domain and its complex with ICAM-1 reveal a shape-shifting pathway for integrin regulation. Cell *112*, 99–111.

Springer, T.A. (1994). Traffic signals for lymphocyte recirculation and leukocyte emigration: the multi-step paradigm. Cell *76*, 301–314.

Stevens, F.J. (1989). Analysis of protein-protein interaction by simulation of small-zone size exclusion chromatography. Stochastic formulation of kinetic rate contributions to observed high-performance liquid chromatography elution characteristics. Biophys. J. *55*, 1155–1167.

Takagi, J., Beglova, N., Yalamanchili, P., Blacklow, S.C., and Springer, T.A. (2001a). Definition of EGF-like, closely interacting modules that bear activation epitopes in integrin β subunits. Proc. Natl. Acad. Sci. USA *98*, 11175–11180.

Takagi, J., Erickson, H.P., and Springer, T.A. (2001b). C-terminal opening mimics "inside-out" activation of integrin α5β1. Nat. Struct. Biol. *8*, 412–416.

Takagi, J., Petre, B.M., Walz, T., and Springer, T.A. (2002). Global conformational rearrangements in integrin extracellular domains in outside-in and inside-out signaling. Cell *110*, 599–611.

Takagi, J., Strokovich, K., Springer, T.A., and Walz, T. (2003). Structure of integrin α5β1 in complex with fibronectin. EMBO J. *22*, 4607–4615.

Takami, M., Herrera, R., and Petruzzelli, L. (2001). Mac-1-dependent tyrosine phosphorylation during neutrophil adhesion. Am. J. Physiol. Cell Physiol. *280*, C1045–C1056.

Vorup-Jensen, T., Ostermeier, C., Shimaoka, M., Hommel, U., and Springer, T.A. (2003). Structure and allosteric regulation of the αXβ2 integrin I domain. Proc. Natl. Acad. Sci. USA *100*, 1873–1878.

Welzenbach, K., Hommel, U., and Weitz-Schmidt, G. (2002). Small molecule inhibitors induce conformational changes in the I domain and the I-like domain of lymphocyte function-associated antigen-1: molecular insights into integrin inhibition. J. Biol. Chem. *277*, 10590–10598.

Xiao, T., Takagi, J., Wang, J.-h., Coller, B.S., and Springer, T.A. (2004). Structural basis for allostery in integrins and binding of ligand-mimetic therapeutics to the platelet receptor for fibrinogen. Nature *432*, 59–67.

Xie, C., Shimaoka, M., Xiao, T., Schwab, P., Klickstein, L.B., and Springer, T.A. (2004). The integrin α subunit leg extends at a Ca2+-dependent epitope in the thigh/genu interface upon activation. Proc. Natl. Acad. Sci. USA *101*, 15422–15427.

Xiong, J.-P., Stehle, T., Diefenbach, B., Zhang, R., Dunker, R., Scott, D.L., Joachimiak, A., Goodman, S.L., and Arnaout, M.A. (2001). Crystal structure of the extracellular segment of integrin αVβ3. Science *294*, 339–345.

Xiong, J.P., Stehle, T., Zhang, R., Joachimiak, A., Frech, M., Goodman, S.L., and Arnaout, M.A. (2002). Crystal structure of the extracellular segment of integrin αVβ3 in complex with an Arg-Gly-Asp ligand. Science *296*, 151–155.

Xiong, J.P., Stehle, T., Goodman, S.L., and Arnaout, M.A. (2004). A novel adaptation of the integrin PSI domain revealed from its crystal structure. J. Biol. Chem. *279*, 40252–40254.

Yang, W., Shimaoka, M., Chen, J.F., and Springer, T.A. (2004a). Activation of integrin β subunit I-like domains by one-turn C-terminal α-helix deletions. Proc. Natl. Acad. Sci. USA *101*, 2333–2338.

Yang, W., Shimaoka, M., Salas, A., Takagi, J., and Springer, T.A. (2004b). Inter-subunit signal transmission in integrins by a receptor-like interaction with a pull spring. Proc. Natl. Acad. Sci. USA *101*, 2906–2911.

Zang, Q., and Springer, T.A. (2001). Amino acid residues in the PSI domain and cysteine-rich repeats of the integrin β2 subunit that restrain activation of the integrin αXβ2. J. Biol. Chem. *276*, 6922–6929.

Supplemental Data

Activation of Leukocyte β_2 Integrins by Conversion from Bent to Extended Conformations

Noritaka Nishida, Can Xie, Motomu Shimaoka, Yifan Cheng, Thomas Walz, and Timothy A. Springer

Supplemental Reference

Saxton, W. O., and Baumeister, W. (1982). The correlation averaging of a regularly arranged bacterial cell envelope protein. J Microsc *127*, 127-138.

Supplementary Table 1

Summary of image classification and averaging

Construct	Condition[1]	Selection[2]	Particles	Classes
Clasped $\alpha_X\beta_2$	None	All	4,435	50
Unclasped $\alpha_X\beta_2$	None	Compact	1,925	50
		Elongated	5,890	100
Clasped $\alpha_L\beta_2$	None	Compact	3,454	100
		Elongated	3,950	100
Unclasped $\alpha_L\beta_2$	None	Compact	1,900	50
		Elongated	5,040	250
Clasped $\alpha_X\beta_2$	XVA	All	5,766	100
Unclasped $\alpha_X\beta_2$	XVA	All	5,029	100
Clasped $\alpha_X\beta_2$	CBR1/2	Elongated	7,502	200
		Compact	690	20
Unclasped $\alpha_X\beta_2$	CBR1/2	All	6,283	300
Clasped $\alpha_X\beta_2$	KIM+XVA	Elongated	4,474	100
		Compact	381	20
Clasped $\alpha_X\beta_2$	CBR1/2+KIM	All	8,860	200

1 XVA: XVA143, CBR1/2: CBR LFA-1/2 Fab, KIM: KIM127 Fab

2 All particles in the same images were segregated into “compact” and “elongated” groups and separately subjected to multireference alignment, or all particles were subjected to multireference alignment.

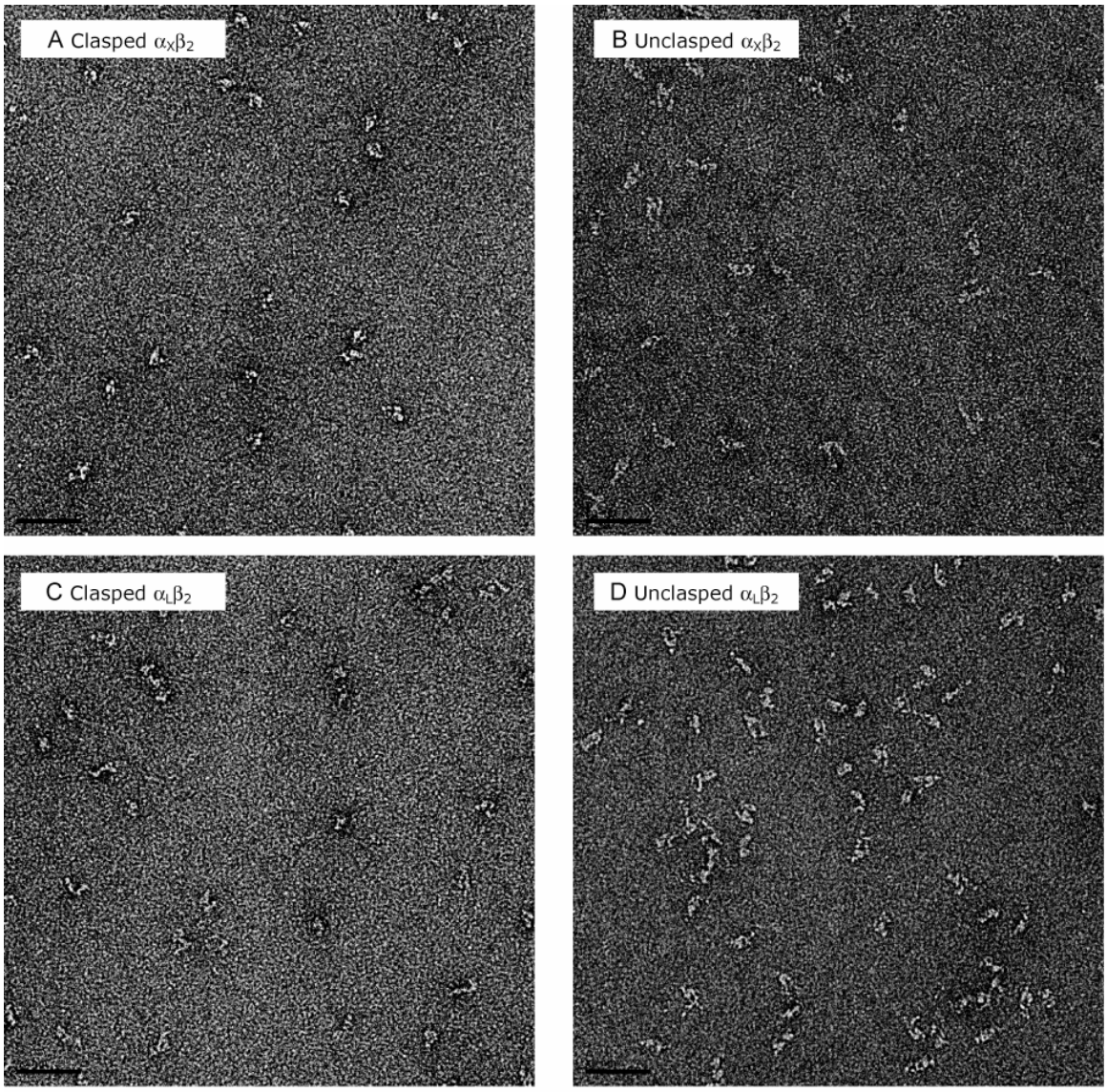

Figure S1. Raw Images

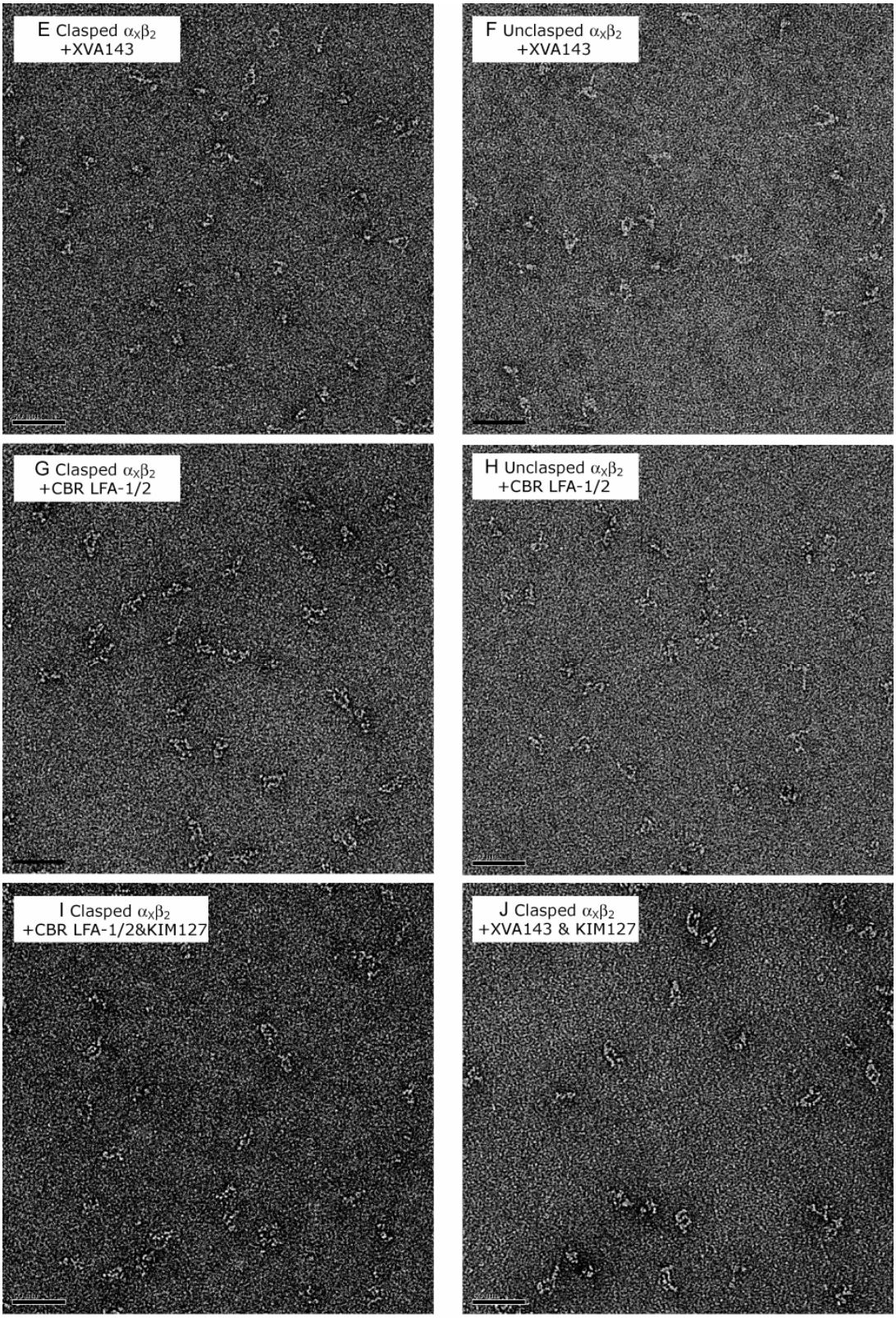

Figure S1. Raw Images (continued)

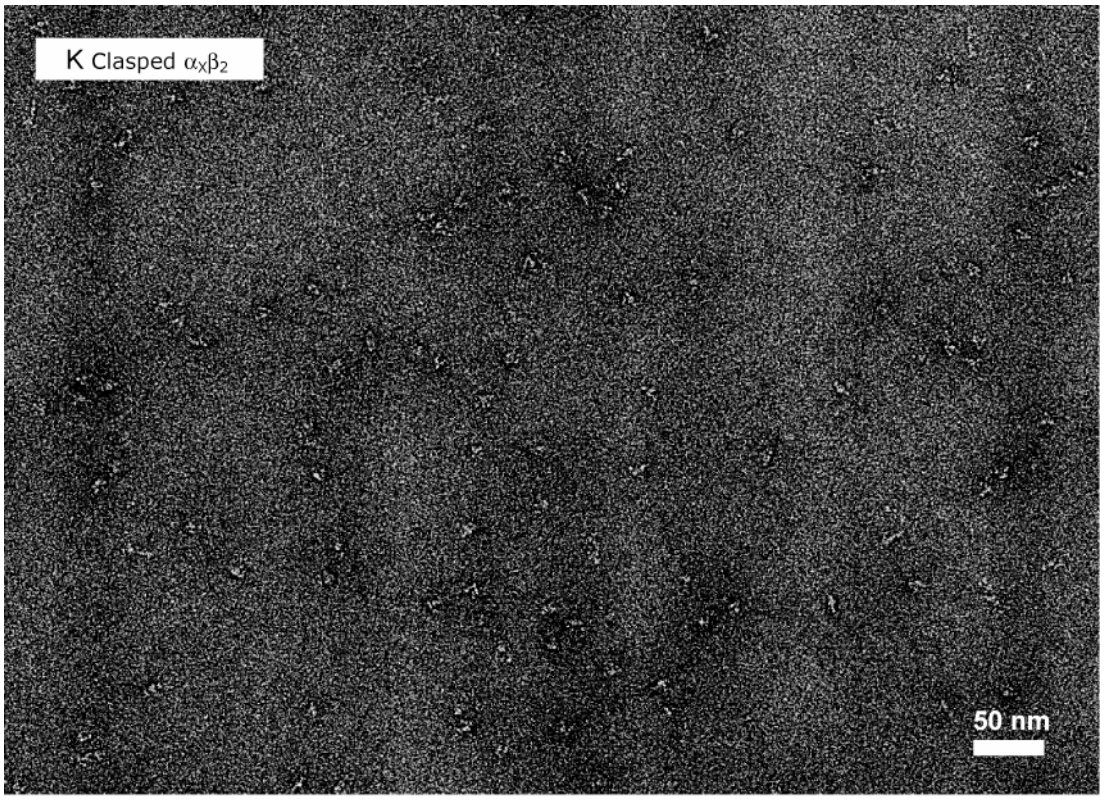

Figure S1. Raw Images (continued)

A-J. One complete, representative, raw CCD image is shown for each integrin preparation. **K.** A representative raw film exposure, which covers a wider area than the CCD images. Bars: 50 nm.

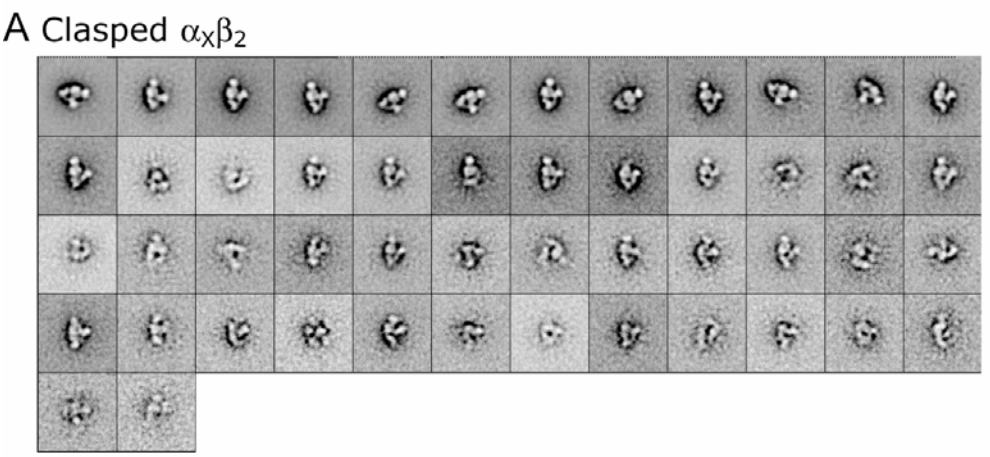

Figure S2. Class Averages

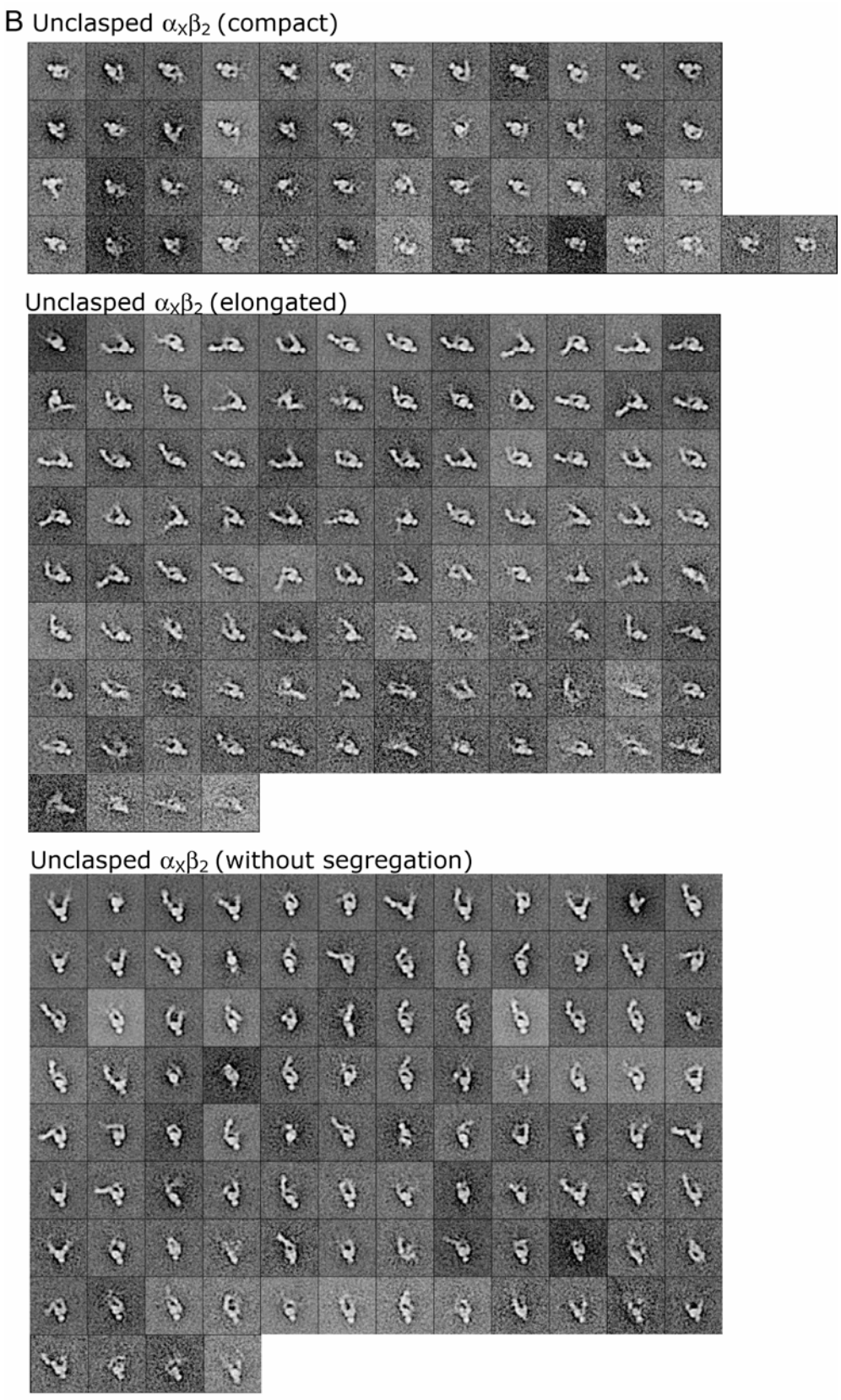

Figure S2. Class Averages (continued)

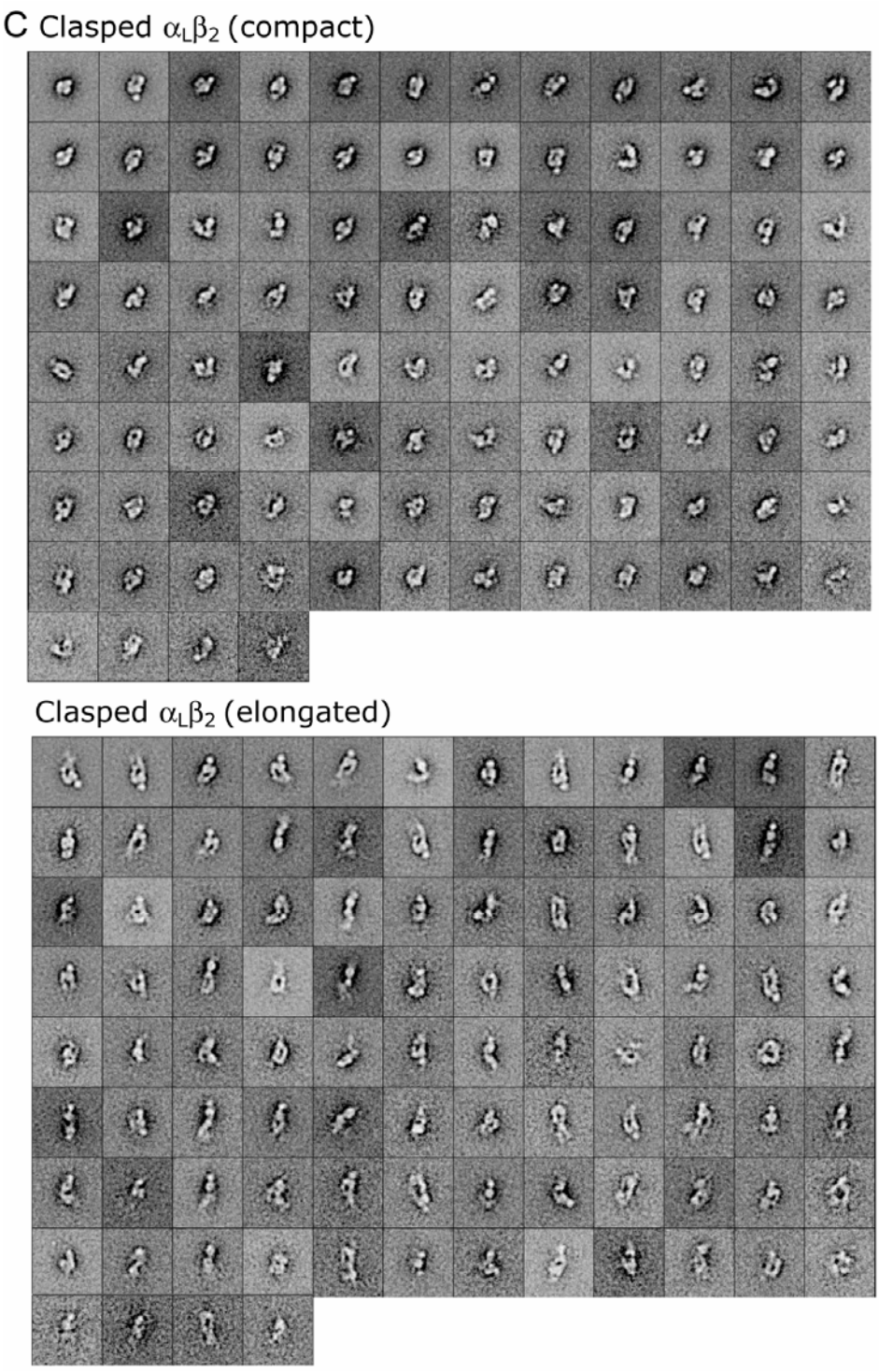

Figure S2. Class Averages (continued)

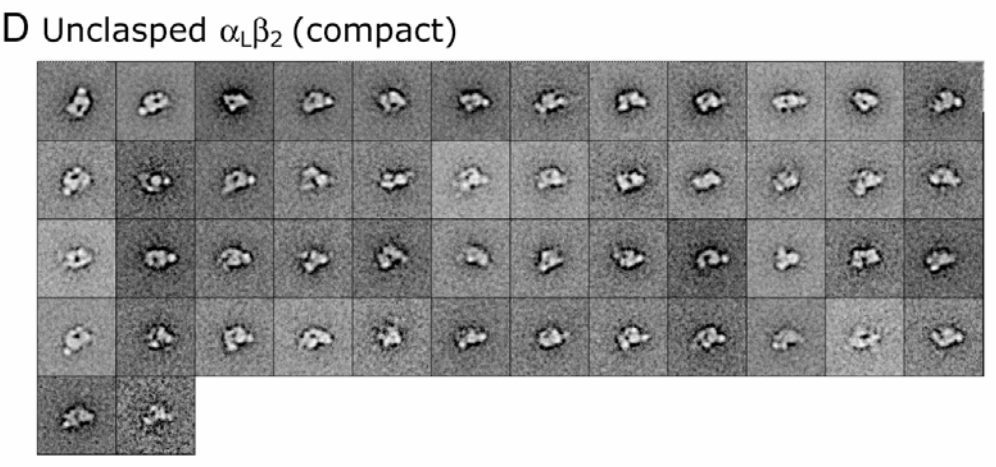

Figure S2. Class Averages (continued)

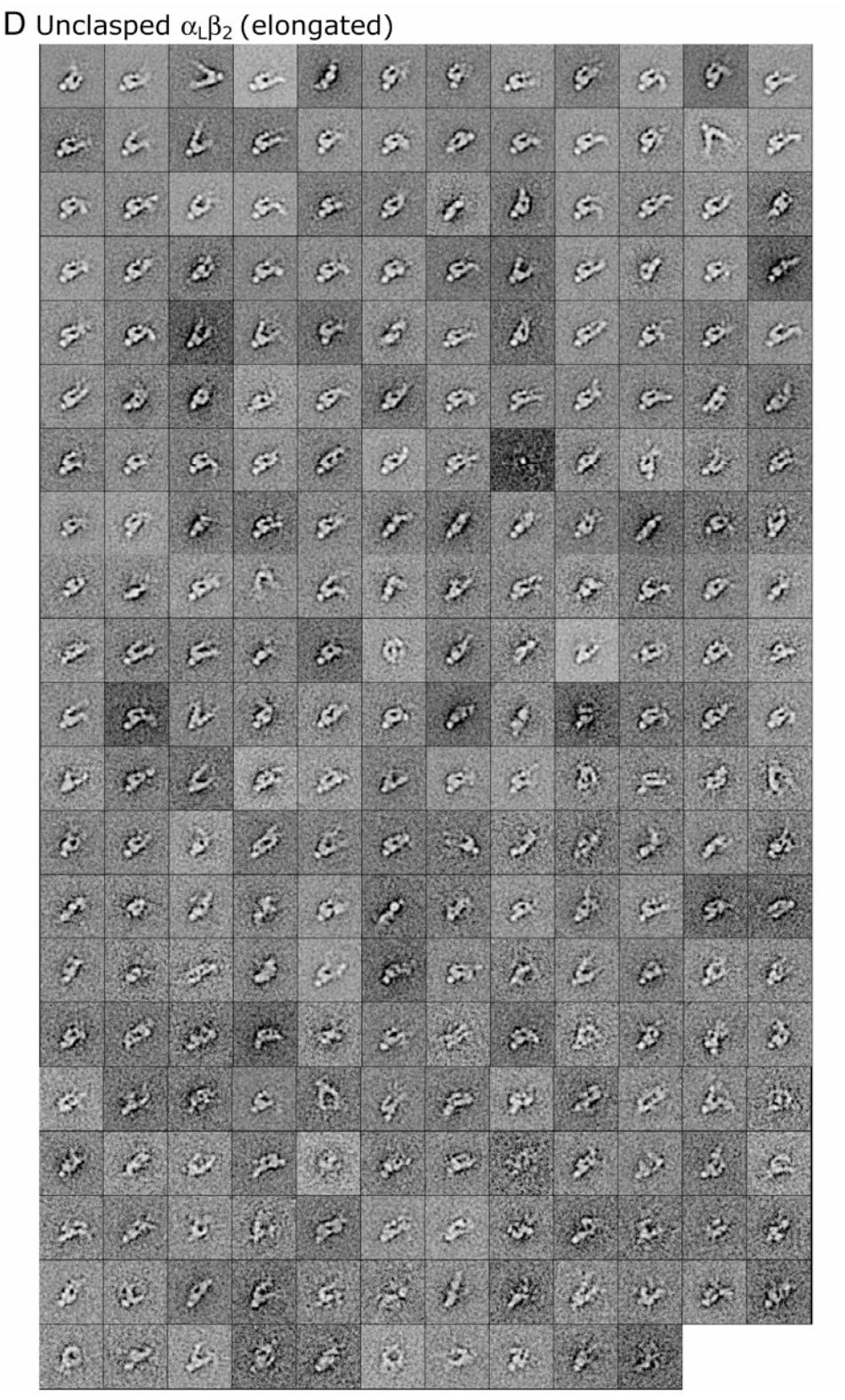

Figure S2. Class Averages (continued)

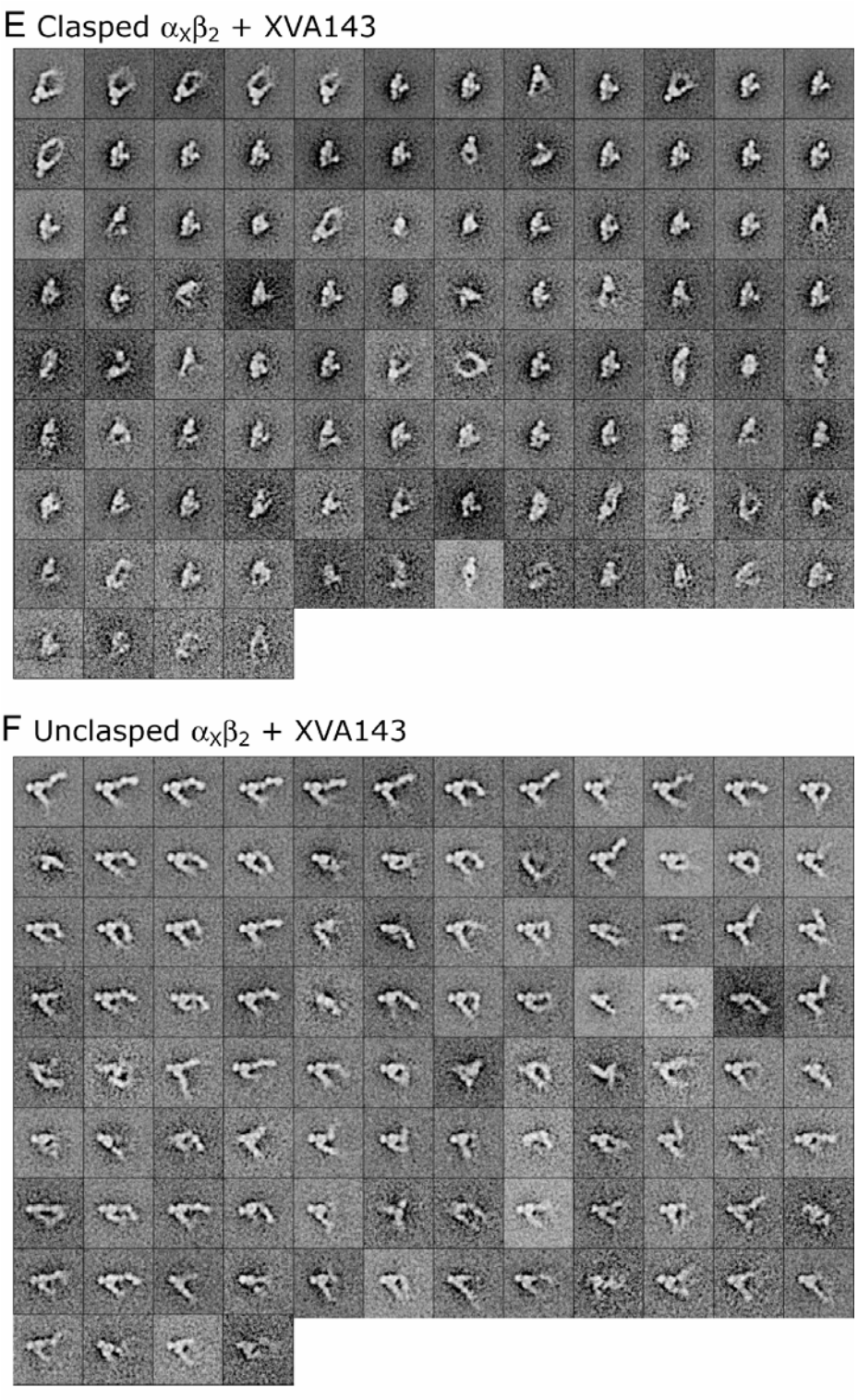

Figure S2. Class Averages (continued)

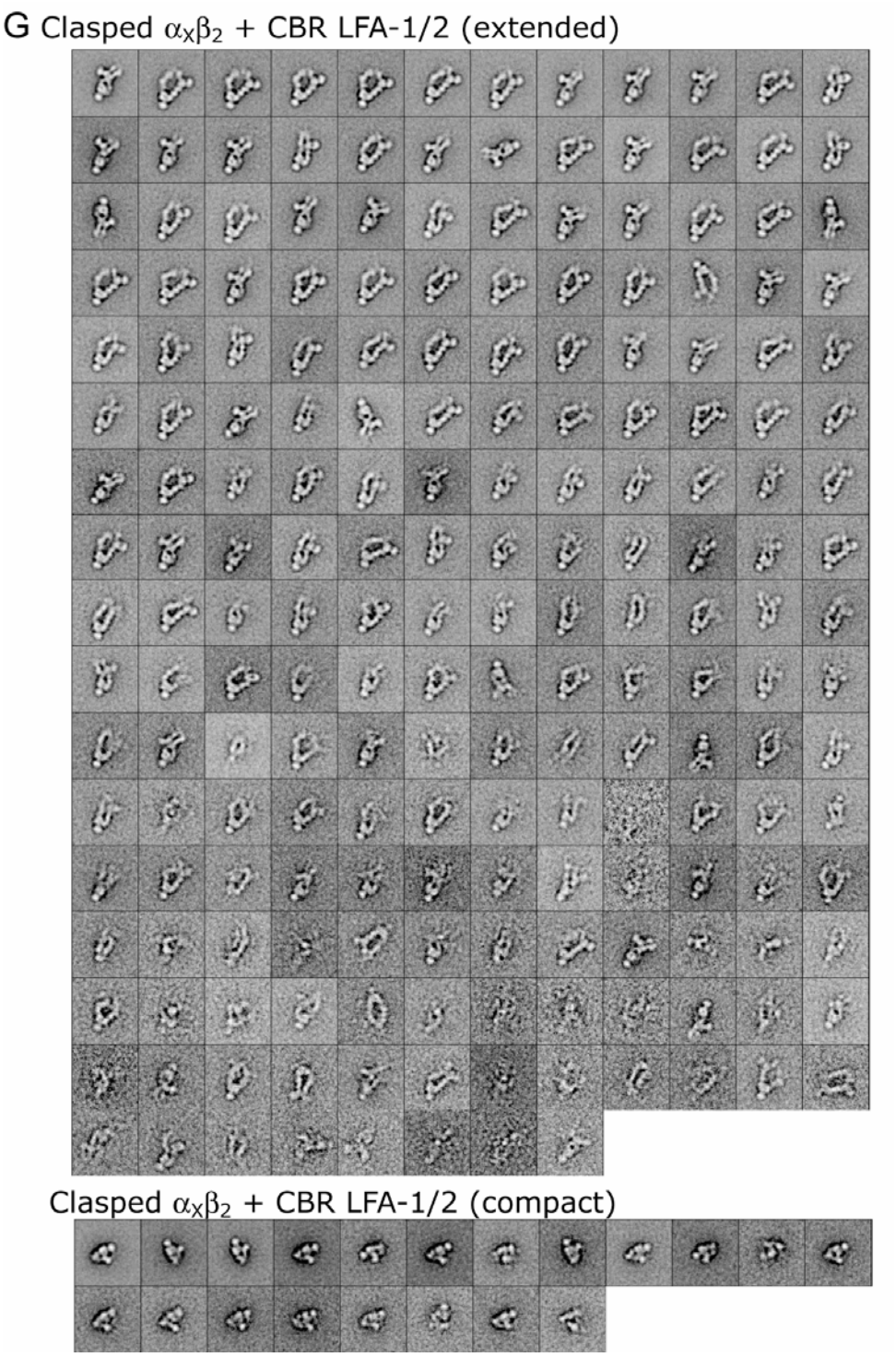

Figure S2. Class Averages (continued)

H Unclasped $\alpha_X\beta_2$ + CBR LFA-1/2

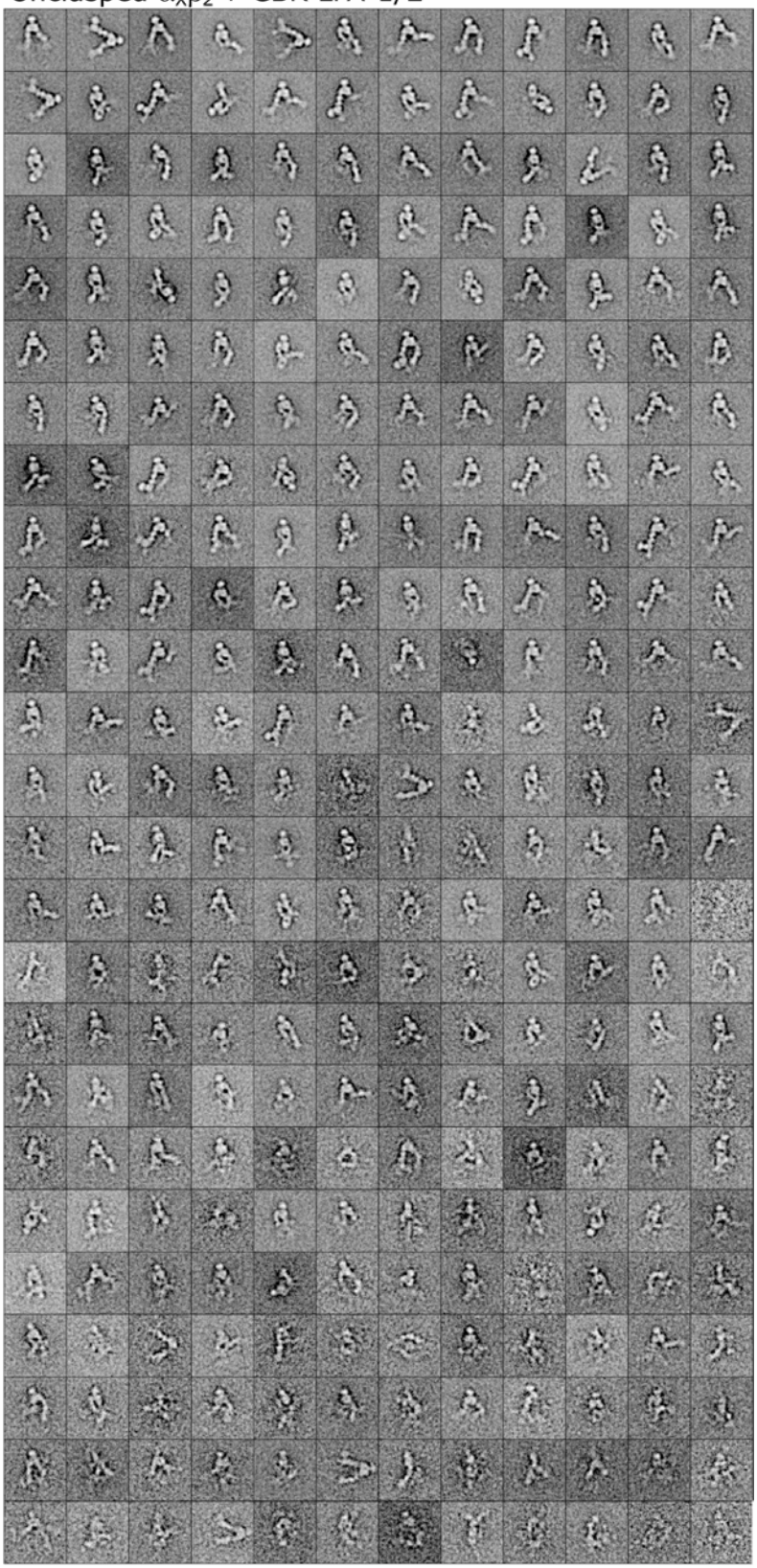

Figure S2. Class Averages (continued)

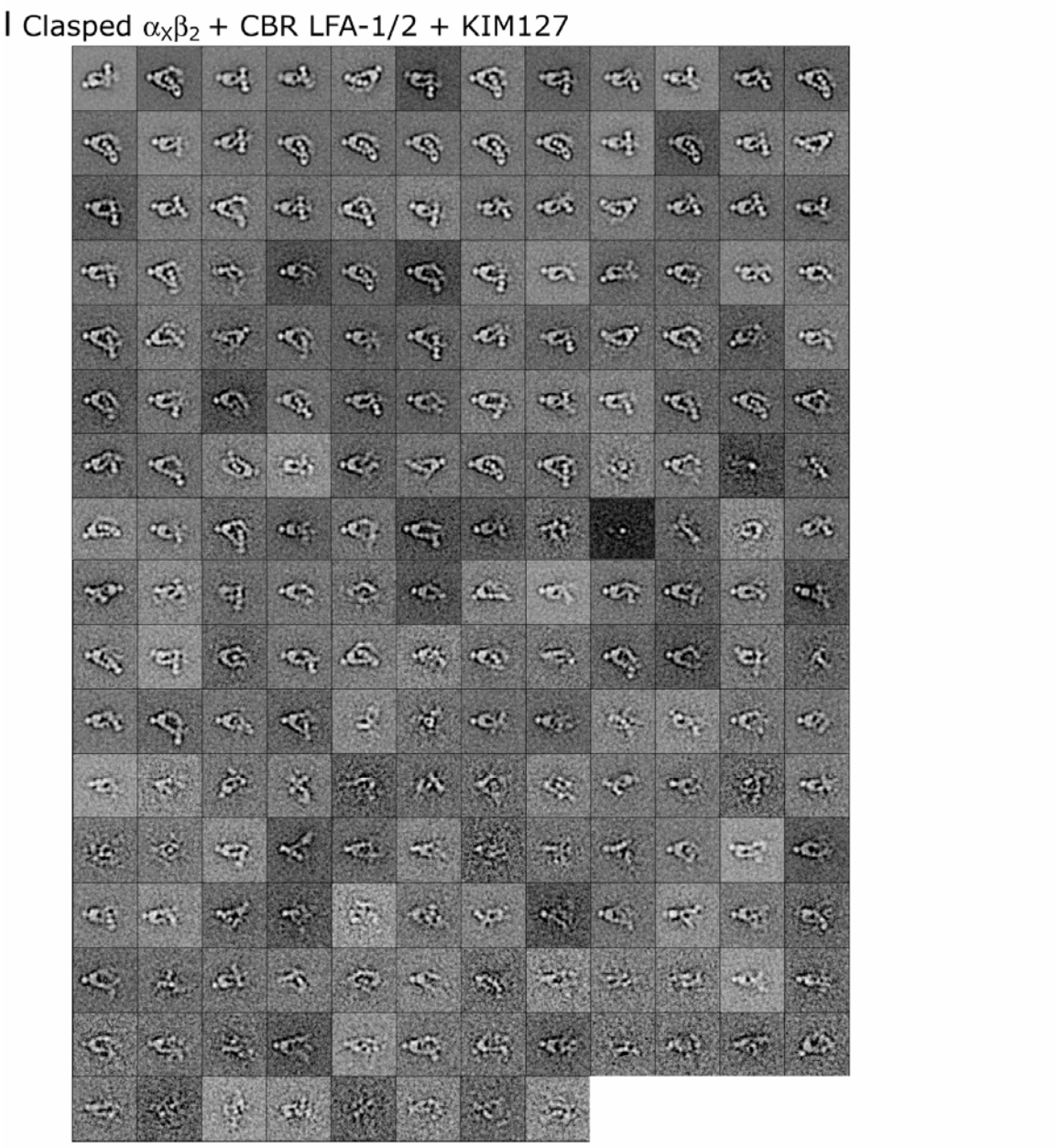

Figure S2. Class Averages (continued)

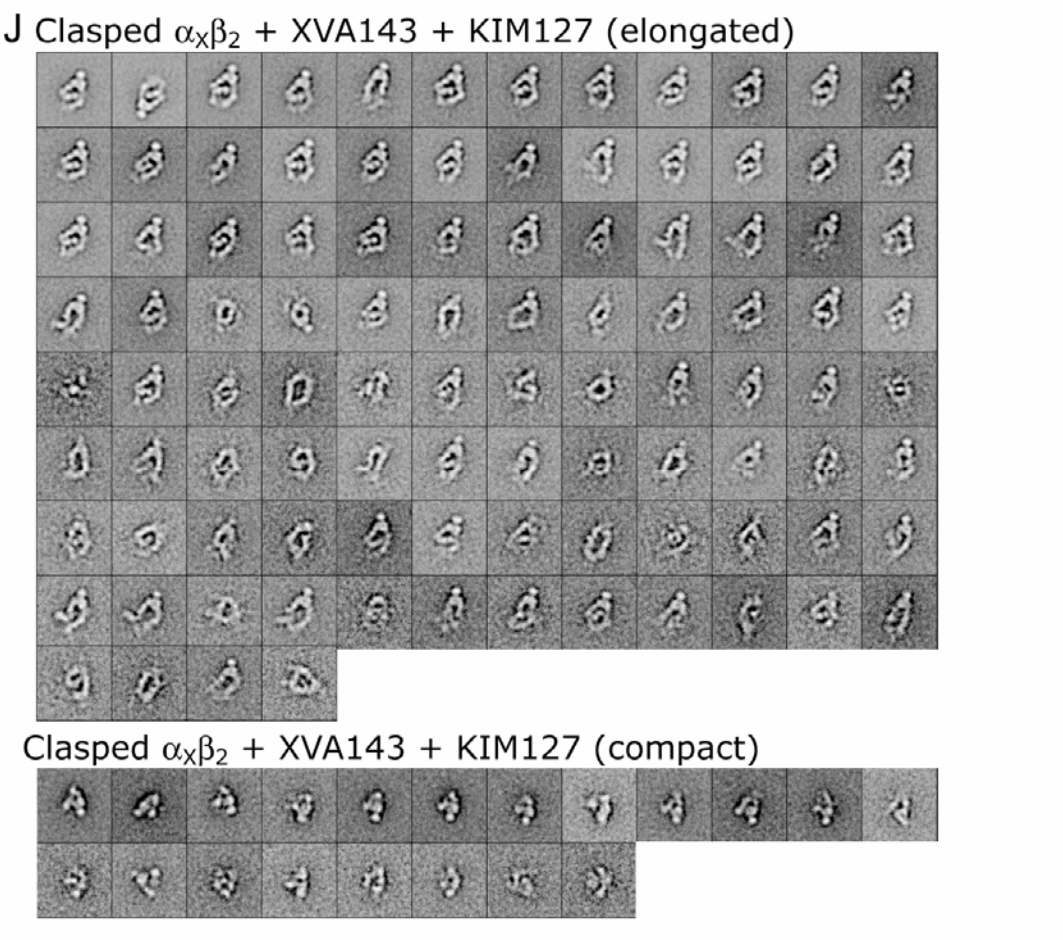

Figure S2. Class Averages (continued)

All 1740 class averages computed in this study, as summarized in Supplementary Table 1, are shown. As described, some class averages were computed separately for compact and elongated particles. The class averages are arranged in order by the number of particles in each class, reading by row from left to right, and from top to bottom row, i.e. the leftmost average in the first row and the rightmost average in the last row are the most and least populous, respectively. Each class average is 40.4 x 40.4 nm.

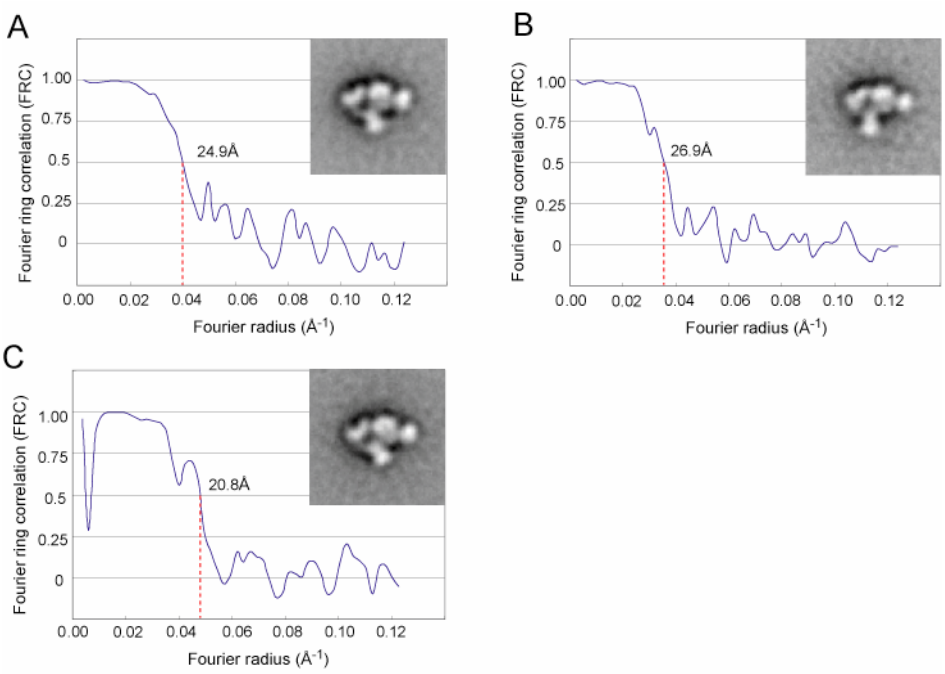

Figure S3. Fourier Ring Correlation

For each representative class average, the particles were randomly apportioned into two equally sized sets, class averages were computed, and the Fourier ring correlation between the two class averages was determined (Saxton and Baumeister, 1982). The resolution is estimated as the radius at which the correlation is 0.5, and ranges between 20 Å and 30 Å.